Article

SOURCE DATA TRANSPARENT PROCESS

EMBO reports

Sinhcaf-dependent histone deacetylation is essential for primordial germ cell specification

Binbin Tao[1,†], Hongling Hu[1,†], Ji Chen[1], Lu Chen[1,2], Daji Luo[1], Yonghua Sun[1], Feng Ge[1], Zuoyan Zhu[1], Vance L Trudeau[3] & Wei Hu[1,2,4,*]

Abstract

Primordial germ cells (PGCs) are the progenitor cells that give rise to sperm and eggs. Sinhcaf is a recently identified subunit of the Sin3 histone deacetylase complex (SIN3A-HDAC). Here, we provide evidence that Sinhcaf-dependent histone deacetylation is essential for germ plasm aggregation and primordial germ cell specification. Specifically, maternal-zygotic *sinhcaf* zebrafish mutants exhibit germ plasm aggregation defects, decreased PGC abundance and male-biased sex ratio, which can be rescued by re-expressing *sinhcaf*. Overexpression of *sinhcaf* results in excess PGCs and a female-biased sex ratio. Sinhcaf binds to the promoter region of *kif26ab*. Loss of *sinhcaf* epigenetically switches off *kif26ab* expression by increasing histone 3 acetylation in the promoter region. Injection of *kif26ab* mRNA could partially rescue the germ plasm aggregation defects in *sinhcaf* mutant embryos. Taken together, we demonstrate a role of Sinhcaf in germ plasm aggregation and PGC specialization that is mediated by regulating the histone acetylation status of the *kif26ab* promoter to activate its transcription. Our findings provide novel insights into the function and regulatory mechanisms of Sinhcaf-mediated histone deacetylation in PGC specification.

Keywords germ plasm; histone deacetylases; kinesin; primordial germ cells; Sinhcaf

Subject Categories Chromatin, Transcription & Genomics; Development; Stem Cells & Regenerative Medicine

DOI 10.15252/embr.202154387 | Received 24 November 2021 | Revised 12 April 2022 | Accepted 14 April 2022 | Published online 9 May 2022

EMBO Reports (2022) 23: e54387

Introduction

Germline stem cells (GSCs), primordial germ cells (PGCs) are established in early development. Specified PGCs migrate to the genital ridge (Raz, 2003; Saitou & Yamaji, 2012), proliferate, and differentiate into spermatogonia and oogonia, which give rise to the gametes—sperm and eggs. Mammalian GSCs help maintain spermatogenesis throughout the lifetime of mature males, but whether females have the capacity to generate new oocytes after birth has until very recently (Martin *et al*, 2019) been highly controversial (Grieve *et al*, 2015). In non-mammalian animals, GSCs persist into adulthood and continue to produce new gametes throughout reproductive life (Marlow, 2015). The survival of species is dependent upon PGCs in sexually reproducing organisms because they are the founder cells for the germline (Cinalli *et al*, 2008). Abnormalities in this developmental process can cause embryonic depletion of germ cells, leading to infertility in the adult (Agoulnik *et al*, 2002).

In *Caenorhabditis elegans*, *Drosophila melanogaster*, *Xenopus laevis*, and the zebrafish *Danio rerio*, PGCs are specified by inheritance of maternal germ plasm during early embryogenesis (Illmensee & Mahowald, 1974; Hird *et al*, 1996; Yoon *et al*, 1997; Lehmann, 2016). The germ plasm is characterized by the presence of germ granules: electron-dense structures that contain specific RNA (e.g., *vasa*, *dead end*, *nanos3*, *dazl* mRNA) and protein (e.g., Buc, Tdrd6a, Oskar) molecules (Houston & King, 2000; Bontems *et al*, 2009; Kistler *et al*, 2018; Krishnakumar *et al*, 2018). Zebrafish germ plasm aggregates into cleavage furrows in cleavage stage embryos (Eno *et al*, 2019). Ablation of germ plasm from cleavage furrows results in a severe reduction in the number of PGCs (Hashimoto *et al*, 2004). Germ plasm thus is both sufficient and necessary for zebrafish PGC specification. Germ plasm accumulation at cleavage furrows requires coordination of microtubules, actin cytoskeletons, and molecular motors (Nair *et al*, 2013; Sinsimer *et al*, 2013), yet how this process is regulated remains poorly understood.

Histone deacetylases (HDACs) catalyze the removal of acetyl residues from core histones and other proteins (Karantzali *et al*, 2008; Dovey *et al*, 2010a; Adams *et al*, 2018). Various critical physiological roles have been assigned to HDACs or histone deacetylation, including those related to signal transduction (Kao *et al*, 1998), cell survival and differentiation (Yeung *et al*, 2004; Dovey *et al*, 2010b), cell cycle regulation (Zhang *et al*, 2000), and cancer development

1 State Key Laboratory of Freshwater Ecology and Biotechnology, Institute of Hydrobiology, The Innovation Academy of Seed Design, Chinese Academy of Sciences, Wuhan, China
2 University of Chinese Academy of Sciences, Beijing, China
3 Department of Biology, University of Ottawa, Ottawa, ON, Canada
4 Qingdao National Laboratory for Marine Science and Technology, Qingdao, China
*Corresponding author. Tel: +86 27 68780051; E-mail: huwei@ihb.ac.cn
†These authors contributed equally to this work

(Li & Seto, 2016), but whether HDACs or histone deacetylation functions in germ plasm aggregation has not been studied.

The HDACs exist in large, multi-subunit protein complexes, and Sinhcaf (SIN3A and HDAC-associated factor, HUGO nomenclature, previously called Fam60a) is a new component of the SIN3A-HDAC complex (Streubel *et al*, 2017), but little is known about its function. The *sinhcaf* gene is found on chromosome 12 in humans and chromosome 4 in zebrafish. The *sinhcaf* gene respectively codes for 221 and 245 amino acid polypeptides in humans and zebrafish, exhibiting high sequence similarity (~80% identity). The earliest *in vitro* studies of Sinhcaf/Fam60a revealed involvement in cell cycle regulation and cell migration (Munoz *et al*, 2012; Smith *et al*, 2012). Genome-wide association studies suggest the involvement of Sinhcaf/Fam60a in type 2 diabetes (Imamura *et al*, 2016). It was shown that Sinhcaf/Fam60a is required for self-renewal of embryonic stem cells (Streubel *et al*, 2017). Sinhcaf/Fam60a regulates gene expression by regulating DNA methylation at a subset of gene promoters in mouse (Nabeshima *et al*, 2018). However, it is not known whether Sinhcaf can regulate biological processes through histone deacetylation. We previously reported that Sinhcafl, a homologous protein of Sinhcaf, is involved in reprogramming of somatic cell nuclear transfer (Luo *et al*, 2009; Hu *et al*, 2018). In this current study, we have investigated whether *sinhcaf* functions in germ plasm aggregation and primordial germ cell specification.

To accomplish this, we have generated viable *sinhcaf* mutant and overexpression zebrafish lines. The maternal-zygotic *sinhcaf* mutants (MZ*sinhcaf*$^{-/-}$) exhibit germ plasm aggregation defects, decreased PGC abundance and male-biased sex ratio, effects that are rescued by *sinhcaf* overexpression. Overexpression of *sinhcaf* results in excess PGCs and a female-biased sex ratio. We report that Sinhcaf-mediated histone deacetylation modulates germ plasm aggregation and subsequent PGC specification in zebrafish. The role of Sinhcaf in germ plasm aggregation and PGC specification is mediated by regulating the histone acetylation status of the *kif26ab* promoter to activate its transcription.

Results

sinhcaf is required for female sexual differentiation in zebrafish

We have established the expression pattern of *sinhcaf* in wild-type zebrafish embryos and adult tissues by semi-quantitative reverse-transcriptase PCR and whole-mount in situ hybridization (WISH). *Sinhcaf* is a maternally expressed gene (Fig 1A) and ubiquitously distributed in embryos and various adult tissues (Fig 1B and C and Appendix Fig S1).

To investigate the role of *sinhcaf* during germ plasm aggregation and PGC specification *in vivo*, a pair of TALENs were designed for the zebrafish *sinhcaf* gene. The TALEN target site of *sinhcaf* was chosen following the ATG start site. The *sinhcaf* heterozygote with 7-bp deletion (−7 bp) was screened out and further used to establish the *sinhcaf*$^{-/-}$ homozygous mutant line (Fig 1D). The *sinhcaf*$^{-/-}$ (−7bp) mutation zebrafish resulted in open reading frame-shift, predicted to generate a truncated protein with only 41 amino acids (Appendix Fig S2A). Real-time quantitative PCR (RT–qPCR) revealed that *sinhcaf* mRNA levels were significantly decreased by 81% ($P = 0.028$) in MZ*sinhcaf*$^{-/-}$ mutant embryos (Fig 1E), indicating a mechanism of nonsense-mediated mRNA decay (Chang *et al*, 2007). Using Tol2 transposon-mediated transgenesis (Appendix Fig S2B), we also generated a transgenic zebrafish line, *Tg(CMV:EGFP;CMV:sinhcaf)* (Fig 1F), which expressed *sinhcaf* ubiquitously. The *sinhcaf* mRNA level was significantly increased by1.5- ($P = 0.009$) and 1.6-fold ($P = 0.009$), respectively, in 10hpf and 24hpf *Tg(CMV:EGFP;CMV:sinhcaf)* embryos as measured by RT–qPCR (Fig 1G). Surprisingly, we found that sex ratio was significantly affected by *sinhcaf* genotype ($F_{3,8} = 29.861$, $P < 0.001$, Fig 1H). Specifically, the percentage of males was 88 ± 0.82% in MZ*sinhcaf*$^{-/-}$ mutant adult fish, significantly higher compared to 57 ± 10% in wild type ($P = 0.032$). In *Tg(CMV:EGFP;CMV:sinhcaf)* adult fish, the percentage of males was only 4.3 ± 3.7%, significantly lower than the percentage of males in the wildtype group ($P = 0.002$). Through exogenous expression of *sinhcaf*, the percentage of males was restored to 45 ± 7% in mutant adult fish, which is not significantly different from wild type ($P = 0.865$) (Fig 1H).

PGC specification is *sinhcaf*-dependent

It is generally recognized that PGC abundance plays a critical role in sexual development (Slanchev *et al*, 2005; Ye *et al*, 2019; Feng *et al*, 2020). Therefore, we investigated the possible role of *sinhcaf* in PGC abundance. We found the number of PGCs were significantly affected by *sinhcaf* genotype in bud stage embryos ($F_{3,36} = 32.125$, $P < 0.001$, Fig 2A–C). Specifically, the number of PGCs stained with *vasa* or *nanos3* probes were significantly decreased by 65% in MZ*sinhcaf*$^{-/-}$ embryos ($P < 0.001$), while significantly increased by 50% in bud stage *sinhcaf* overexpressing embryos ($P = 0.001$) (Fig 2A–C), compared to wild type. Exogenous expression of *sinhcaf* increased the number of PGCs by 1.9-fold ($P < 0.001$) (Fig 2B and C) and rescued the loss of PGCs in bud stage MZ*sinhcaf*$^{-/-}$ embryos. Similar results were observed in dome stage, 21-somites and 24hpf embryos (Fig 2A–C).

The *sinhcaf*$^{-/-}$ mutants were crossed with the *Tg(piwil1:EGFP)* line that expresses green fluorescent protein (GFP) in PGCs. Their progeny were raised to adulthood and intercrossed to establish a *sinhcaf* homozygous mutant line expressing GFP in PGCs, i.e., MZ*sinhcaf*$^{-/-}$; *Tg(piwil1:EGFP)*. *In vivo* 3D confocal imaging revealed a significant decrease in the number of PGCs ($P < 0.001$) (Figs 2D and E, and EV1A) which are labeled with GFP in the zebrafish genital ridge of the MZ*sinhcaf*$^{-/-}$ mutants. The number of Vasa-positive PGCs was decreased in 24phf MZ*sinhcaf*$^{-/-}$ embryos compared to wild type (Fig EV1B). The expression of PGCs marker genes was determined using RT–qPCR. As shown in Fig 2F, the mRNA levels of *vasa*, *dnd* and *nanos3* were significantly decreased by 40, 79 and 80% in bud stage MZ*sinhcaf*$^{-/-}$ mutant embryos, respectively, compared to wild type.

Germ plasm aggregation is defective in maternal-zygotic *sinhcaf* mutant embryos

We hypothesized that decreased maternal germ plasm components or defective germ plasm aggregation may be responsible for PGC specification defects in MZ*sinhcaf*$^{-/-}$ mutants. As shown in Fig 3A the level of germ plasm stained by the *vasa* probe was decreased in cleavage furrows of 4-cell stage MZ*sinhcaf*$^{-/-}$ embryos, compared

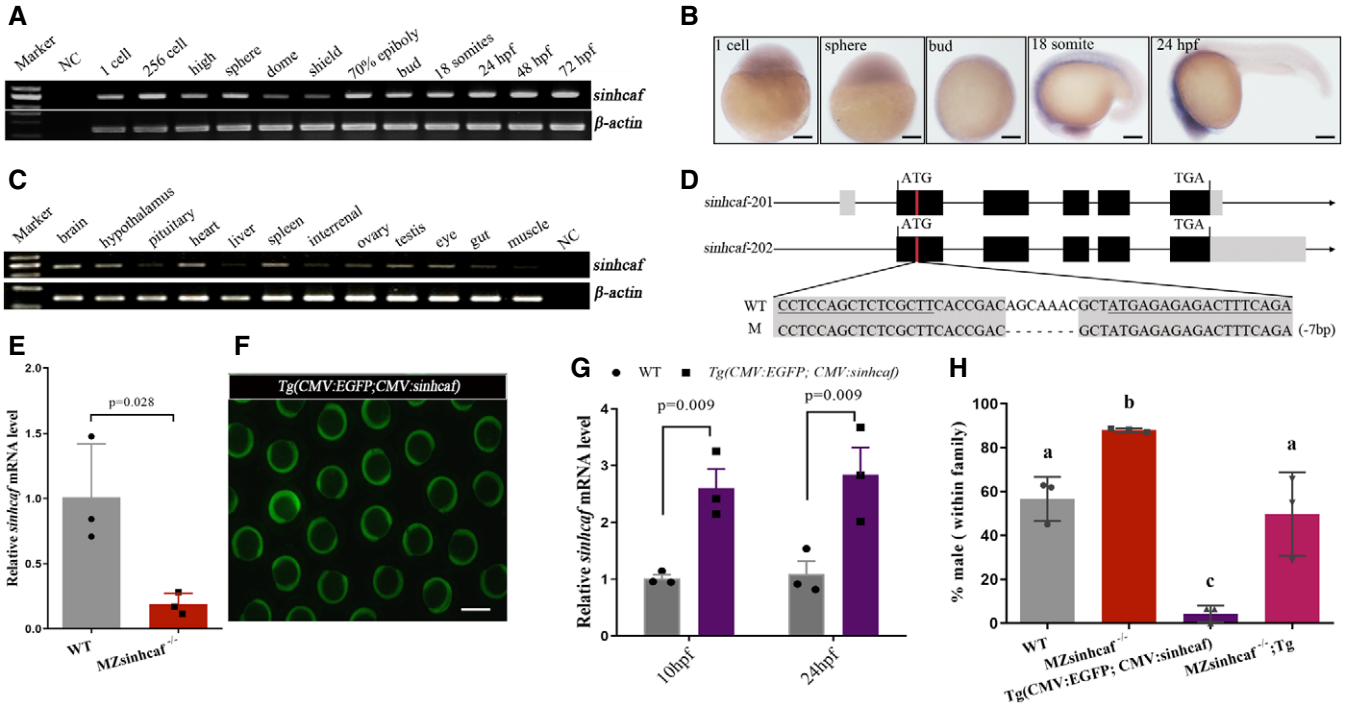

Figure 1. *sinhcaf* is required for female sexual differentiation in zebrafish.

A RT–PCR analysis for temporal expression of *sinhcaf* mRNA during embryogenesis and early larval developmental stages. NC indicates the no template control.

B Time-course expression of *sinhcaf* revealed by whole-mount *in situ* hybridization. Scale bars, 100 μm.

C RT–PCR analysis for spatial expression of *sinhcaf* mRNA in adult tissues.

D The location of the TALEN-binding sites (underlined) on zebrafish *sinhcaf* gene and mutant line of TALEN-targeted *sinhcaf* alleles.

E Relative mRNA level of *sinhcaf* in bud stage WT and MZ*sinhcaf*$^{-/-}$ mutant embryos as measured by RT–qPCR. Data shown are mean ± SEM (n = 3, biological replicates). Statistical analysis was performed using unpaired two-tailed Student's t-test.

F Fluorescence microscopy of 10hpf *Tg(CMV:EGFP;CMV:sinhcaf)* zebrafish embryos. Scale bar, 400 μm.

G Relative mRNA level of *sinhcaf* in 10hpf or 24hpf WT and *Tg(CMV:EGFP;CMV:sinhcaf)* embryos as measured by RT–qPCR. Data shown are mean ± SEM (n = 3, biological replicates). Statistical analysis was performed using 2-way ANOVA followed by Holm-Sidak post hoc test.

H Percentage of male zebrafish in WT (n = 274), MZ*sinhcaf*$^{-/-}$ (n = 166), *Tg(CMV:EGFP;CMV:sinhcaf)* (n = 158) and MZ*sinhcaf*$^{-/-}$;*Tg(CMV:EGFP;CMV:sinhcaf)* (n = 135) adult zebrafish. Data shown are mean ± SEM (n = the number of fish analyzed). Statistical analysis was performed using one-way ANOVA followed by Tukey's post hoc test. The different letters (a, b, c) indicate a significant difference between the means, $P < 0.05$.

Source data are available online for this figure.

to wild type. In contrast, the maternal mRNA levels of *vasa*, *dnd*, *nanos3*, *dazl* and *buc* in whole unfertilized eggs were not affected in the MZ*sinhcaf*$^{-/-}$ line (Fig 3B). This indicates that germ plasm aggregation was disrupted in MZ*sinhcaf*$^{-/-}$ embryos, but not the expression levels of key germ plasm components.

To further investigate germ plasm aggregation, mRNA for the live imaging biomarker Buc-GFP (Campbell *et al*, 2015; Riemer *et al*, 2015) was injected into wild type or MZ*sinhcaf*$^{-/-}$ mutant 1-cell embryos. As shown in Fig 3C and D, the Buc-GFP signal was significantly decreased by 41.6% in MZ*sinhcaf*$^{-/-}$ cleavage furrows ($P < 0.001$), compared to wild type. In contrast, the level of total Buc-GFP determined by Western blotting was unchanged in 4-cell stage MZ*sinhcaf*$^{-/-}$ zebrafish embryos compared to wild type (Fig 3E and F).

Loss of *sinhcaf* leads to an increase in histone 3 acetylation in full-grown (FG) follicles

To investigate the interaction of zebrafish Sinhcaf with the core components of the SIN3-HDAC complex, co-immunoprecipitation was performed using HEK293T cells that were transiently transfected with both Sinhcaf-GFP expression vector and plasmids expressing HA-Sin3a, HA-Hdac1 or HA-Sap18. Western blot analysis of Sinhcaf-GFP immunoprecipitations showed that Sinhcaf-GFP precipitated core components of the SIN3-HDAC complex (Fig 4A–C).

We conducted RT–qPCR to measure *sinhcaf* mRNA level in zebrafish follicles. The levels of *sinhcaf* gradually increased from the PG stage to maximal levels at the FG stage (Figs 4D and EV2A). The *sinhcaf* mRNA level was significantly higher in FG stage follicles, compared to other stage follicles. To examine whether *sinhcaf* was expressed in oocytes, the denuded oocytes and follicular cell layers were separated from FG follicles (Fig EV2B). We found that *sinhcaf* was expressed in both denuded oocytes and follicular cell layers (Fig EV2C).

To investigate whether Sinhcaf is required for histone deacetylation in zebrafish follicles, the level of acetyl-histone H3 (K9) was determined in wild type or *sinhcaf*$^{-/-}$ zebrafish primary growth (PG), previtellogenic (PV), early vitellogenic (EV), mid vitellogenic (MV) and FG follicles by western blotting. As shown in Fig 4E and G, the

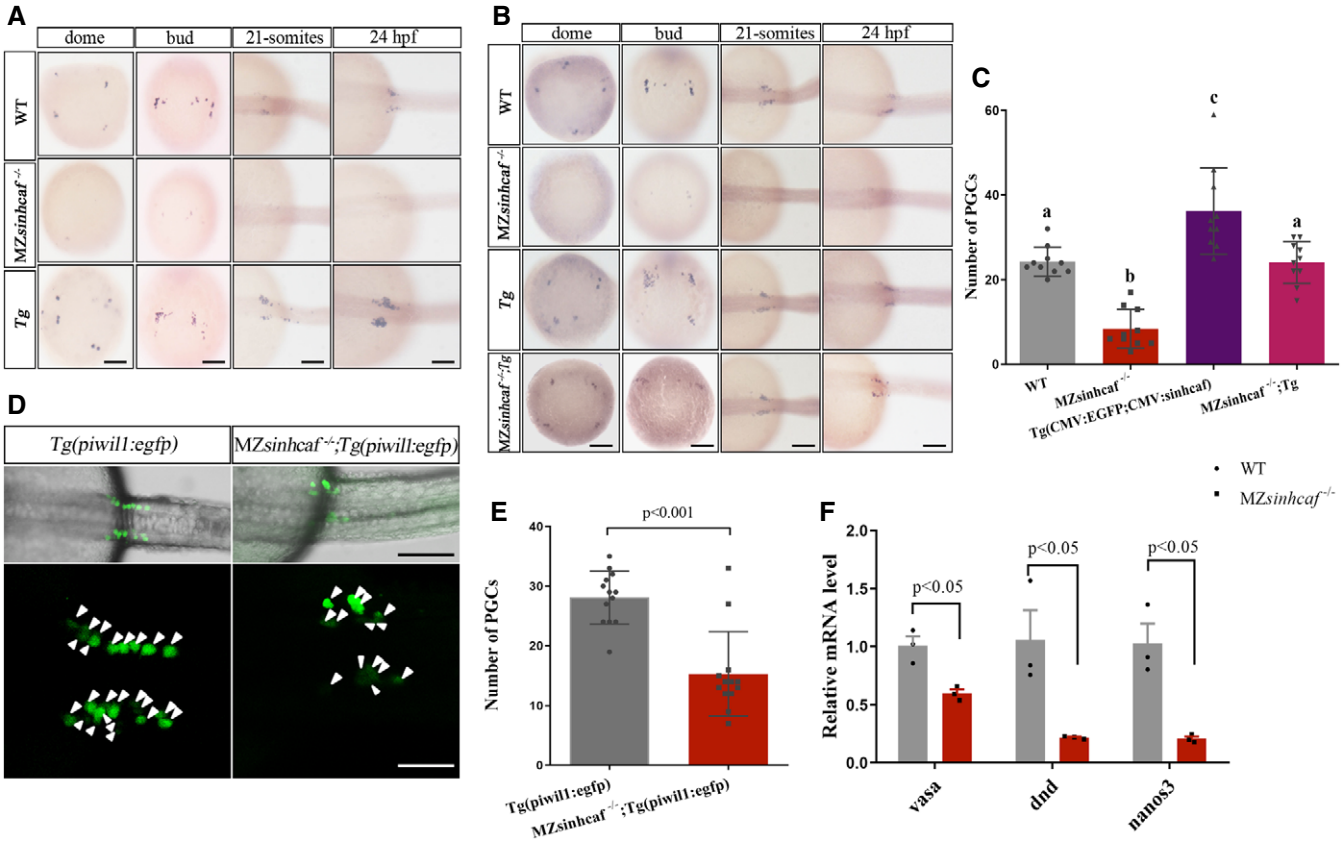

Figure 2. PGC specification is *sinhcaf*-dependent in zebrafish.

A, B Whole-mount *in situ* hybridization was performed in WT, MZ*sinhcaf*$^{-/-}$, *Tg(CMV:EGFP;CMV:sinhcaf)* and MZ*sinhcaf*$^{-/-}$;*Tg(CMV:EGFP;CMV:sinhcaf)* zebrafish embryos with PGCs markers *nanos3* (A) and *vasa* (B). Scale bars, 100 μm.

C Quantitative analysis of PGCs in bud stage WT, MZ*sinhcaf*$^{-/-}$, *Tg(CMV:EGFP;CMV:sinhcaf)* and MZ*sinhcaf*$^{-/-}$;*Tg(CMV:EGFP;CMV:sinhcaf)* zebrafish embryos. Data shown are mean ± SEM (n = 10, the number of embryos analyzed). Statistical analysis was performed using one-way ANOVA followed by Tukey's post hoc test. The different letters (a, b, c) indicate a significant difference between the means, $P < 0.05$.

D Maximal intensity projection of a confocal z-stack of 24hpf *Tg(piwil1:EGFP)* and MZ*sinhcaf*$^{-/-}$; *Tg(piwil1:EGFP)* zebrafish embryos, dorsal views. Arrowheads point to PGCs. Scale bars, 100 μm.

E Quantitative analysis of PGCs in 24hpf *Tg(piwil1:EGFP)* and MZ*sinhcaf*$^{-/-}$; *Tg(piwil1:EGFP)*zebrafish embryos. Data shown are mean ± SEM (n = 13, the number of embryos analyzed). Statistical analysis was performed using unpaired two-tailed Student's t-test.

F Relative mRNA level of *vasa*, *dnd* and *nanos3* in 24 hpf WT and MZ*sinhcaf*$^{-/-}$ mutant embryos, respectively, as measured by RT–qPCR. Data shown are mean ± SEM (n = 3, biological replicates). Statistical analysis was performed using 2-way ANOVA followed by Holm-Sidak post hoc test.

level of acetyl-histone H3 (K9) gradually increased from wild-type PG to MV stage follicles, and significantly decreased by 84% in wild-type FG stage follicles ($P < 0.001$), compared to wild-type MV stage follicles. Decreased acetyl-histone H3 (K9) in FG stage follicles may be related to increased *sinhcaf* expression at the same stage (Figs 4D and EV2A). In *sinhcaf*$^{-/-}$ zebrafish follicles, the level of acetyl-histone H3 (K9) also gradually increased from PG to MV stage follicles. While different from wild-type FG stage follicles, the level of acetyl-histone H3 (K9) was not significantly ($P = 0.714$) decreased in *sinhcaf*$^{-/-}$ FG stage follicles compared to *sinhcaf*$^{-/-}$ MV stage follicles (Fig 4F and H).

To further analyze the role of Sinhcaf in histone deacetylation, the level of acetyl-histone H3 (K9) was examined in *sinhcaf*$^{-/-}$ and wild-type follicles at the same stage. It was shown that the level of acetyl-histone H3 (K9) was not affected in *sinhcaf*$^{-/-}$ EV (Fig 4I and M) or MV (Fig 4J and N) stage follicles, compared to wild-type follicles at the same stage respectively. While the level of acetyl-histone H3 (K9) was significantly increased by 2.7-fold ($P = 0.04$) in *sinhcaf*$^{-/-}$ FG stage follicles compared to wild-type FG stage follicles (Fig 4K and O). The levels of acetyl-histone H3 (Lys18) and acetyl-histone H4 (K5) were also assessed in *sinhcaf*$^{-/-}$ and wild-type FG stage follicles by western blotting. As shown in Fig 4L and P, the level of acetyl-histone H3 (K18) was significantly increased by 4-fold ($P = 0.039$), while the level of acetyl-histone H4 (K5) was not affected in *sinhcaf*$^{-/-}$ FG stage follicles (Fig 4L and Q), compared to wild-type FG stage follicles.

Genes related to microtubule functions were downregulated in *sinhcaf* mutant FG follicles and eggs

We investigated the landscape of gene transcription and whether transcription of genes involved in germ plasm aggregation was

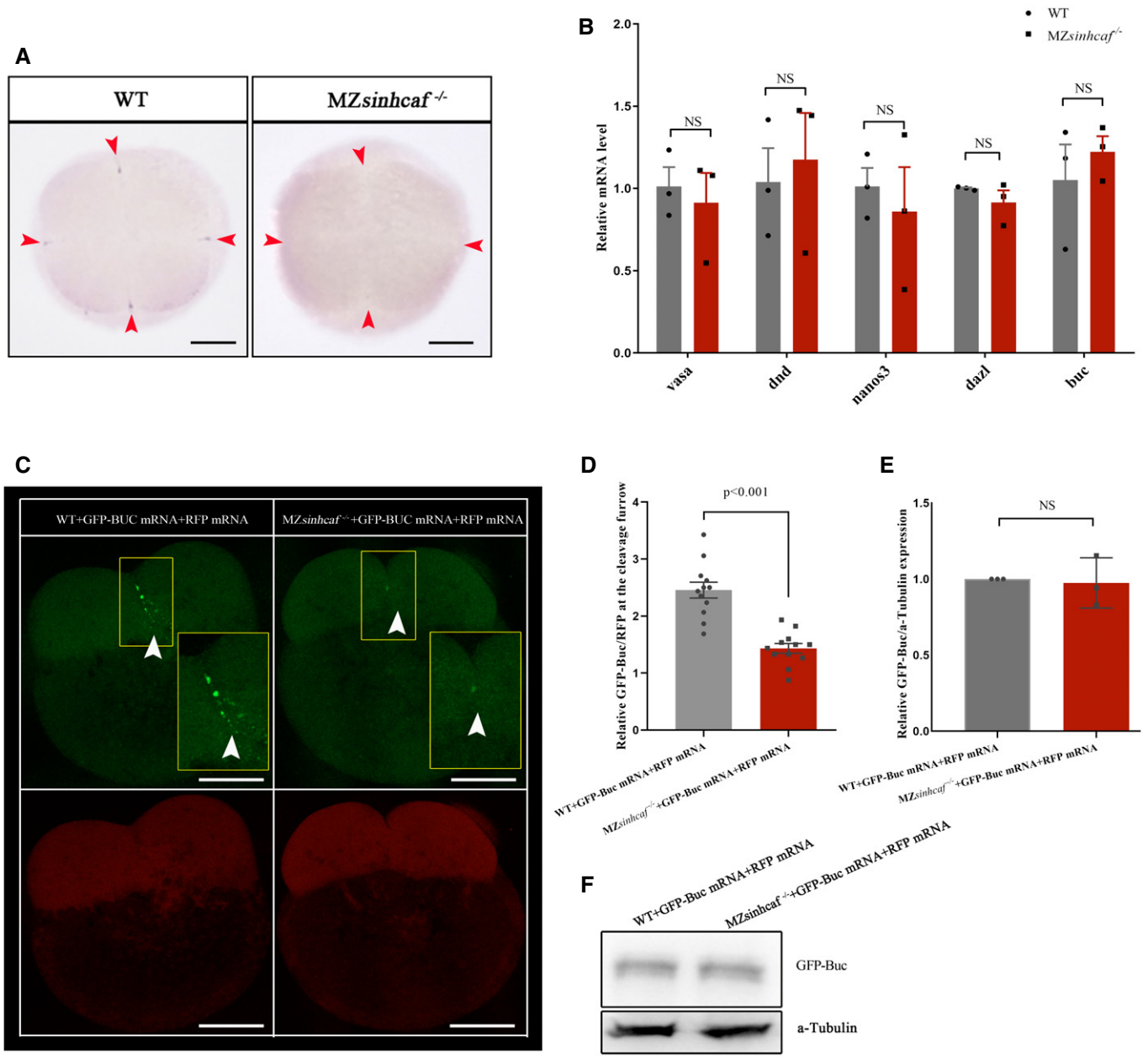

Figure 3. Germ plasm aggregation was disrupted in *sinhcaf* mutant embryos.

A Whole-mount in situ hybridization was performed in 4-cell stage WT, MZ*sinhcaf*$^{-/-}$ zebrafish embryos with germ plasm marker *vasa*. Red arrowheads point to cleavage furrows in the 4-cell embryos. Scale bars, 100 μm.

B Relative mRNA levels of germ plasm genes *vasa*, *dnd*, *nanos3*, *dazl* and *buc* in WT and MZ*sinhcaf*$^{-/-}$ mutant eggs, respectively, as measured by RT–qPCR. Data shown are mean ± SEM (n = 3, biological replicates). Statistical analysis was performed using 2-way ANOVA followed by the Holm-Sidak post hoc test; NS, no significant difference.

C Maximal intensity projection of a confocal z-stack of 4-cell stage WT and MZ*sinhcaf*$^{-/-}$ zebrafish embryos injected with GFP-Buc and RFP mRNA. White arrowheads point to cleavage furrows of 4-cell embryos. Scale bars, 100 μm.

D Relative GFP-Buc density at the cleavage furrow of 4-cell stage WT and MZ*sinhcaf*$^{-/-}$ zebrafish embryos injected with GFP-Buc and RFP mRNA. Statistical analysis was performed using unpaired two-tailed Student's t-test. Data shown are mean ± SEM (n = 12, the number of embryos analyzed).

E Statistical analysis of the relative levels of GFP-Buc/a-Tubulin. Data shown are mean ± SEM (n = 3, biological replicates). Statistical analysis was performed using one-way ANOVA followed by Tukey's post hoc test.

F Western blots for GFP-Buc expression in 4-cell stage WT and MZ*sinhcaf*$^{-/-}$ zebrafish embryos injected with GFP-Buc and RFP mRNA.

Source data are available online for this figure.

affected in *sinhcaf* mutant FG follicles with upregulated acetyl-histone H3. Transcriptome sequencing (RNA-seq) analysis uncovered that 1,238 genes were upregulated, 923 genes were downregulated in *sinhcaf* mutant FG follicles, compared to wild-type FG follicles (Fig 5A). Loss of *sinhcaf* in mature eggs resulted in upregulation of 904 genes, and downregulation of 911 genes (Fig 5B). Downregulated genes in *sinhcaf* mutant FG follicles and eggs were classified by gene ontology (GO) analysis, then the top 30 GO terms with highest -$\log_{10}$P values were screened out, and at least two downregulated genes were included in each biological processes, cellular components or molecular function term. As shown in Figs 5C and EV3A and B, microtubules and microtubule-based processes were included in the top 30 GO terms. Further, we reconfirmed transcriptome analysis results by RT–qPCR and found genes *kif26ab*

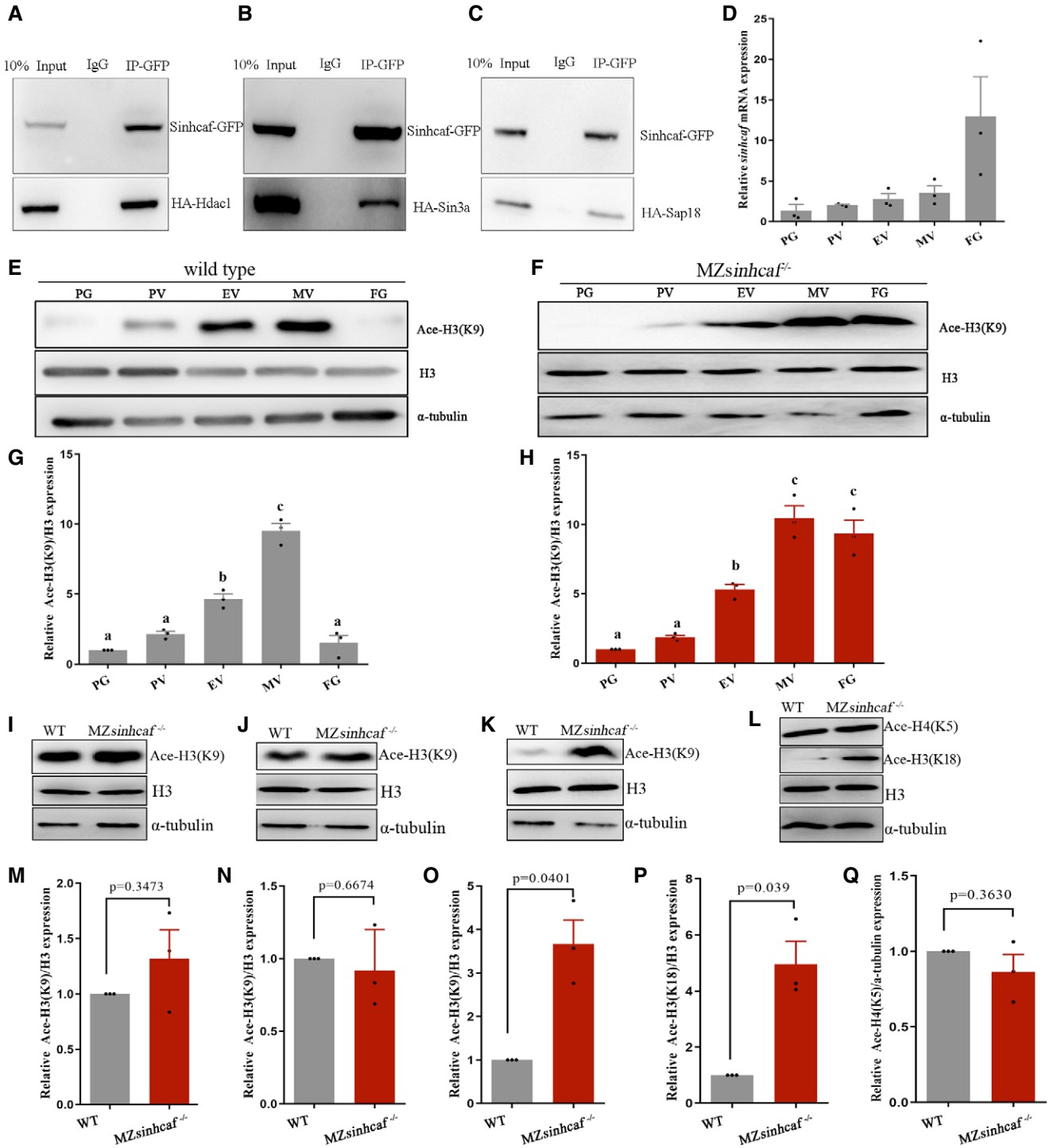

Figure 4.

Figure 4. Loss of Sinhcaf leads to an increase in histone 3 acetylation of FG follicles.

A–C Co-immunoprecipitation of zebrafish Sinhcaf-GFP with HA-Hdac1 (A), HA-Sin3a (B) or HA-Sap18 (C) in HEK293Tcells transfected with both Sinhcaf-GFP and HA-Hdac1 (A), HA-Sin3a (B) or HA-Sap18 (C) plasmids.

D Relative mRNA level of *sinhcaf* in zebrafish PG, PV, EV, MV, and FG follicles was measured using RT–qPCR. Data shown are mean ± SEM (n = 3, biological replicates).

E, F Western blots for acetyl-histone H3 (K9) (Ace-H3-K9), histone H3 in WT (E) or MZ*sinhcaf*$^{-/-}$ (F) PG, PV, EV, MV and FG follicles. α-tubulin was used as a loading control.

G, H Statistical analysis of the relative levels of Ace-H3-K9 in WT (G) or MZ*sinhcaf*$^{-/-}$ (H) PG, PV, EV, MV and FG follicles. Data shown are mean ± SEM (n = 3, biological replicates). Statistical analysis was performed using one-way ANOVA followed by Tukey's post hoc test. The different letters (a, b, c) indicate a significant difference between the means, $P < 0.05$.

I–K Western blots for Ace-H3-K9 and H3 in WT and MZ*sinhcaf*$^{-/-}$ EV (I), MV (J), and FG (K) follicles. α-tubulin was used as a loading control.

L Western blots for Ace-H4-K5, Ace-H3-K18, and H3 in WT and MZ*sinhcaf*$^{-/-}$ FG follicles. α-tubulin was used as a loading control.

M–O Statistical analysis of the relative levels of Ace-H3-K9I n WT and MZ*sinhcaf*$^{-/-}$ EV (M), MV (N) and FG (O) follicles. Data shown are mean ± SEM (n = 3, biological replicates). Statistical analysis was performed using unpaired two-tailed Student's t-test.

P, Q Statistical analysis of the relative levels of Ace-H3-K18 (P) and Ace-H4-K5 (Q) in WT and MZ*sinhcaf*$^{-/-}$ FG follicles. Data shown are mean ± SEM (n = 3, biological replicates). Statistical analysis was performed using unpaired two-tailed Student's t-test.

Data information: EV, early vitellogenic stage (early stage III); FG, full-grown stage (late-stage III); MV, mid vitellogenic stage (mid -stage III); PG, primary growth (stage I); PV, previtellogenic stage (stage II).
Source data are available online for this figure.

(microtubule-based process), *kif5bb* (microtubule-based process), *eml1, dnal1, myo15aa,* and *tuba8l2* (all included in GO term microtubule) were indeed significantly downregulated in *sinhcaf* mutant FG follicles and mature eggs (Figs 5D and EV3C). As reported previously (Hashimoto *et al*, 2004; Theusch *et al*, 2006; Sinsimer *et al*, 2013), microtubules are implicated in germ plasm accumulation at cleavage furrows. Microtubules were labeled with α-tubulin antibody and germ plasm aggregates were labeled with phospho-non-muscle myosin II (p-NMII) antibody. Double-color whole mount immunofluorescence results indicated germ plasm aggregation was disrupted while the structure of microtubule remained normal in *sinhcaf* mutant 2-cell embryo (Fig 5E). Sinhcaf mutation significantly decreased the transcript levels of some microtubule-related genes. Downregulation of these genes may be closely related to the level of acetylation of histone 3. The structure of microtubules remained normal in *sinhcaf* mutant. These data imply the failure of germ plasm accumulation in *sinhcaf* mutants was not caused by defects of microtubule generation.

The role of Sinhcaf in germ plasm aggregation and PGC specialization is mediated by the kinesin Kif26ab

Our RNA-seq and RT–qPCR results revealed that mRNA levels of the kinesins *kif26ab* and *kif5bb* were significantly decreased in *sinhcaf* mutant FG stage follicles and mature eggs. Kinesins are critical for microtubule-dependent transport of germ plasm components in *Drosophila*, *Xenopus* and zebrafish (Robb *et al*, 1996; Zimyanin *et al*, 2008; Campbell *et al*, 2015): Kif26ab is the member of kinesin family 11. To investigate whether the transcription of *kif26ab* is directly regulated by Sinhcaf, ChIP-qPCR was conducted to determine if a Sinhcaf-GFP fusion protein could bind to transcriptional regulatory region of *kif26ab* gene using walking primers along with *kif26ab*-promoter (Fig 6A). As shown in Fig 6B, Sinhcaf could bind to the promoter region of *kif26ab* covered by primer sets 4 and 5. To determine whether loss of *sinhcaf* affected the epigenetic status of the *kif26ab* gene, we performed ChIP assays for acetyl-histone H3 (K9) and acetyl-histone H3 (K18) using specific anti- acetyl-histone H3 antibodies. This revealed that loss of *sinhcaf* increased both acetyl-histone H3 (K9) and acetyl-histone H3 (K18) in the *kif26ab* promoter region with primer set 4 and 5 (Fig 6C and D). Acetyl-histone H3 (K9) ChIP-Seq was conducted to further confirm that loss of *sinhcaf* increases the histone acetylation in the *kif26ab* promoter region. As shown in Fig 6E, *sinhcaf* mutation resulted in the increase of acetyl-histone H3 (K9) occupancy in the *kif26ab* promoter region. We further investigated whether Sinhacf could activate the transcription of *kif26ab* using HEK193T cells harboring a luciferase reporter cassette under the control of the *kif26ab* promoter. Overexpression of *sinhcaf* significantly increased luciferase expression from the *kif26ab* reporter cassette (Fig 6F). Bisulfite sequencing of the promoter regions of *kif26ab* revealed no significant differences in methylation status between WT and *sinhcaf*$^{-/-}$ MV or FG follicles (Appendix Fig S3A and B). These data thus indicate that Sinhcaf directly binds to the promoters of *kif26ab* to activate its transcription by modulating histone acetylation status.

To determine whether decreased maternal mRNA levels of *kif26ab* or *kif5bb* resulted in defective germ plasm aggregation in MZ*sinhcaf*$^{-/-}$ embryos, morpholinos were designed to block the translation of *kif26ab* and *kif5bb* mRNA (Appendix Fig S4A–C). After *kif26ab* knockdown, the number of PGCs was significantly decreased by 29% in the genital ridge ($P < 0.001$) (Fig 7A and B), which is similar to the phenotype observed in MZ*sinhcaf*$^{-/-}$ embryos. The *kif5bb* knockdown did not affect the number of PGCs in the genital ridge (Appendix Fig S5A and B). Furthermore, we co-injected Buc-GFP mRNA + RFP mRNA + *kif26ab* MO into 1-cell embryos and found that the Buc-GFP signal was significantly decreased by 38% ($P = 0.003$) or 41.9% ($P < 0.001$) in cleavage furrows, compared to Buc-GFP mRNA + RFP mRNA + Control MO co-injected or Buc-GFP mRNA + RFP mRNA co-injected embryos (Fig 7C and D). The level of total Buc-GFP was unchanged in 4-cell stage embryos injected with Buc-GFP mRNA + RFP mRNA + *kif26ab* MO, compared to embryos injected with Buc-GFP mRNA + RFP mRNA + Control MO or Buc-GFP mRNA + RFP mRNA (Fig 7E and F). To confirm that the role of Sinhcaf in germ plasm aggregation is mediated by Kif26ab, we co-injected Buc-GFP mRNA + RFP mRNA + *kif26ab* mRNA into 1-cell MZ*sinhcaf*$^{-/-}$ embryos. The Buc-GFP signal was increased by 40.1% in MZ*sinhcaf*$^{-/-}$ embryos through *kif26ab* mRNA injection ($P = 0.012$) (Fig 7G and H). In contrast, the level of total Buc-GFP

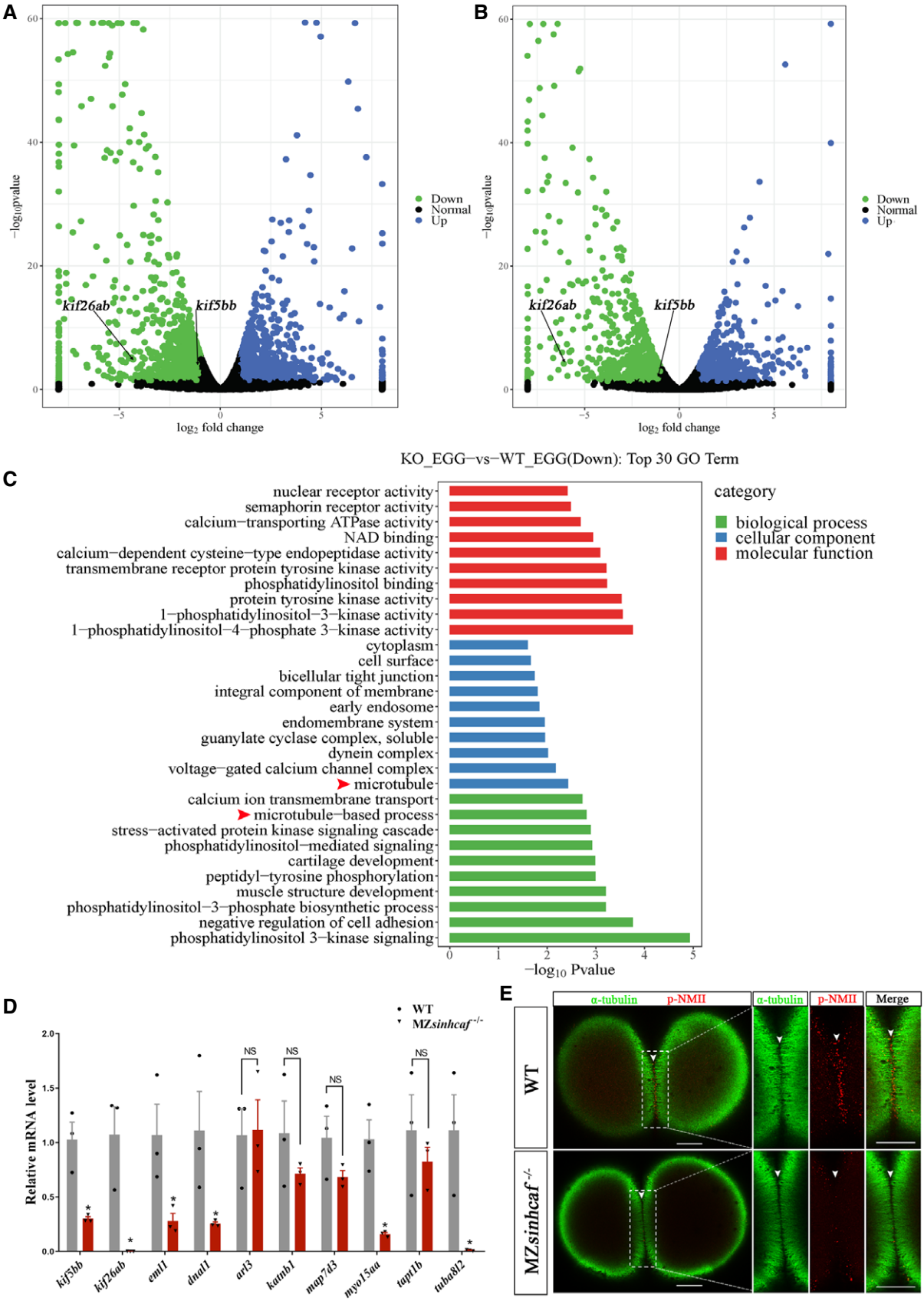

Figure 5.

Figure 5. Genes related to microtubules and microtubule-based processes were downregulated in *sinhcaf* mutant FG follicles and eggs.

A, B Volcano plots showing the relative abundances of transcripts in WT and MZ*sinhcaf*$^{-/-}$ FG follicles (A) or mature eggs (B). Transcripts were differentially expressed if $P < 0.05$ and fold-change > 2 in MZ*sinhcaf*$^{-/-}$ FG follicles or mature eggs compared to WT.

C Annotations for the gene ontology (GO) terms biological process (green), cellular component (blue), molecular function (red) terms were performed for differentially expressed genes in WT and MZ*sinhcaf*$^{-/-}$ mature eggs. Ten GO terms (at least two genes in each term) with highest value of -$\log_{10}$P value are listed in each category. Red arrowheads point to GO term microtubule.

D Significantly downregulated genes related to microtubule and microtubule-based process in *sinhcaf* mutant mature eggs, revealed by transcriptome analysis, are reconfirmed by independent qRT–PCR analysis. Data shown are mean ± SEM ($n = 3$, biological replicates). Statistical analysis was performed using 2-way ANOVA followed by Holm-Sidak post hoc test, *$P < 0.05$. NS, no significant difference.

E Maximal intensity projection of a confocal z-stack for α-tubulin and phospho-non-muscle myosin II (p-NMII) in 2-cell WT and MZ*sinhcaf*$^{-/-}$ *mutant* embryos using whole-mount immunohistochemistry. White arrowheads point to cleavage furrows of 2-cell embryos. Scale bars, 100 μm.

was unchanged in 4-cell stage wild type or MZ*sinhcaf*$^{-/-}$ embryos injected with Buc-GFP mRNA + RFP mRNA or Buc-GFP mRNA + RFP mRNA + *kif26ab* mRNA (Fig 7I and J). Injections with *kif26ab* mRNA thus partially rescues the decreased Buc-GFP signal in cleavage furrows of MZ*sinhcaf*$^{-/-}$ embryos.

Discussion

We have demonstrated that Sinhcaf-dependent histone deacetylation functions in germ plasm aggregation and subsequent PGC specification. Our findings are significant for two main reasons. Firstly, we provide evidence that Sinhcaf-mediated histone deacetylation is critical for germ plasm aggregation and PGC specification. Secondly, we revealed that the essential role of Sinhcaf in germ plasm aggregation and PGC specification is mediated by regulating the histone acetylation status of the *kif26ab* promoter to activate its transcription.

Our study indicates that mutations of maternal-zygotic *sinhcaf* leads to decreased PGCs number in dome stage, bud stage, 21-somites and 24hpf embryos, meanwhile, *sinhcaf* overexpression increased the number of PGCs at these stages. Thus it was demonstrated that zebrafish PGC specialization is *sinhcaf*-dependent. We found maternal-zygotic sinhcaf zebrafish mutants exhibited a male-biased sex ratio. While overexpression of sinhcaf results in a female-biased sex ratio. It has been previously reported that PGC abundance is critical for sex differentiation in zebrafish (Slanchev *et al*, 2005; Feng *et al*, 2020). In zebrafish, individuals with a small number or without PGCs result in later male development, while individuals with a high PGC number have an increased propensity for the female fate (Tzung *et al*, 2015; Ye *et al*, 2019). We found that he number of PGCs was significantly decreased in MZ*sinhcaf*$^{-/-}$ embryos, while significantly increased in *sinhcaf* overexpressing embryos. These data thus indicate the role of *sinhcaf* in sex differentiation is via modulation of PGC specification. In zebrafish, four PGC clusters, each containing about four cells, are found at the dome stage, then PGCs begin to migrate towards the future gonad through 80% epiboly stage, bud stage, 8-somite, 21 somite, and some other stages, finally reaching the genital ridge at 24hpf (Yoon *et al*, 1997; Raz, 2003). Zebrafish PGCs are specified by the inheritance of maternal germ plasm (Hashimoto *et al*, 2004). Germ plasm aggregation is an essential step for PGC specialization: germ plasm gradually accumulates in cleavage furrows during cleavage stage, germ plasm aggregates determine PGC specification (Hashimoto *et al*, 2004; Eno *et al*, 2019). Surprisingly little is known about how the germ plasm aggregation process is regulated. We have shown the maternal mRNA levels of germ plasm components were not affected in MZ*sinhcaf*$^{-/-}$ mutant fish, while germ plasm aggregation was disrupted in MZ*sinhcaf*$^{-/-}$ cleavage stage embryos. Thus, Sinhcaf is a newly identified factor essential for germ plasm aggregation and PGC specialization.

Although histone deacetylation has been reported to play significant roles in many biological processes (Akiyama *et al*, 2006; Matsuda *et al*, 2011; Barber *et al*, 2012; Eskandarian *et al*, 2013), the function of histone deacetylation during germ plasm aggregation remains unknown. Sinhcaf is a new component of histone deacetylase complexes (Streubel *et al*, 2017; Nabeshima *et al*, 2018), which catalyze the removal of acetyl residues from core histones and other proteins (Karantzali *et al*, 2008; Dovey *et al*, 2010a; Adams *et al*, 2018). We found zebrafish Sinhcaf interacted with the core components of SIN3-HDAC complex. The level of *sinhcaf* mRNA was highest in FG stage follicles. In animals, zygotic transcription is not yet activated in early embryonic cleavage (Dosch *et al*, 2004; Lee *et al*, 2014) and the process of germ plasm aggregation is regulated by maternal RNA and protein (Bontems *et al*, 2009; Sinsimer *et al*, 2013; Colozza & De Robertis, 2014; Campbell *et al*, 2015). Maternal factors accumulate during oogenesis. Oocyte maturation is the final step of oogenesis, FG is the final stage of oocyte development before maturation. We demonstrated that loss of Sinhcaf resulted in increased acetylation level of histone 3 in zebrafish FG follicles. Combined with the results that germ plasm aggregation and PGC specialization is defective in MZ*sinhcaf*$^{-/-}$ embryos, we infer that Sinhcaf-mediated histone deacetylation may be related to germ plasm aggregation and PGC specialization.

Reduced histone acetylation has been shown to promote the formation of higher order and more condensed chromatin, which inhibits gene transcription. Thus, the histone deacetylase complexes have mostly been defined within the context of transcriptional repression (Hassig *et al*, 1997; Adams *et al*, 2018). Progress in recent years indicates that the histone deacetylase complex also functions in transcriptional activation (Kurdistani *et al*, 2002; Wang *et al*, 2009; Jamaladdin *et al*, 2014). Our transcriptomic analysis shows that the number of genes with increased expression was roughly equivalent with the number of genes with reduced expression in *sinhcaf* mutant FG follicles or mature eggs, compared to wild type. This suggests that Sinhcaf may have dual roles in both transcriptional activation and repression. Both the transcriptomic and RT–qPCR results showed the level of *kif26ab* transcripts was significantly decreased in *sinhcaf* mutant FG follicles and mature eggs, compared to wild type. Sinhcaf can directly bind to the transcriptional regulatory region of *kif26ab*. Loss of *sinhcaf* increased both acetyl-histone H3 (K9) and acetyl-histone H3 (K18) levels in the promoter region of *kif26ab*. The results of the luciferase-promoter assay

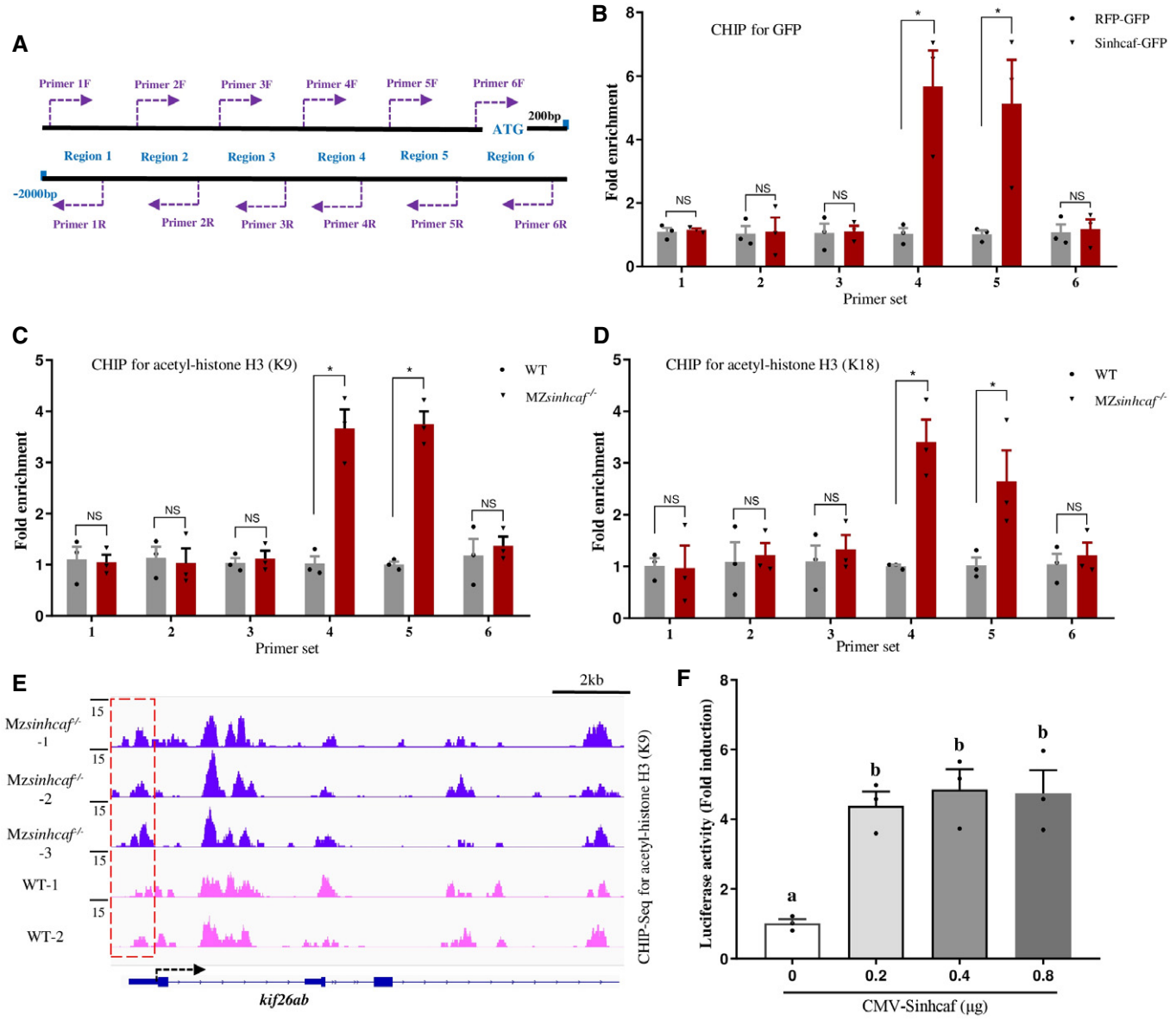

Figure 6. Loss of *sinhcaf* increases acetyl-histone H3 (K9) and acetyl-histone H3 (K18) levels in the promoter region of *kif26ab*.

A Six pairs of walking primers were designed along the *kif26ab* promoter.

B ChIP assay was performed to evaluate whether Sinhcaf binds to the *kif26ab* promoter directly in zebrafish. Data shown are mean ± SEM (n = 3, biological replicates), *P < 0.05. Statistical analysis was performed using 2-way ANOVA followed by Holm-Sidak post hoc test.

C, D The ChIP assay was performed to determine the influence of MZ*sinhcaf* $^{-/-}$ mutation on acetyl-histone H3 (K9) and acetyl-histone H3 (K18) of the *kif26ab* promoter in zebrafish. Data shown are mean ± SEM (n = 3, biological replicates), *P < 0.05. Statistical analysis was performed using 2-way ANOVA followed by Holm-Sidak post hoc test.

E IGV track view of acetyl-histone H3 (K9) occupancy on the *kif26ab* gene region in MZ*sinhcaf* mutant and wild-type zebrafish embryos. The increased ChIP-seq peaks are highlighted with red dashed rectangle.

F HEK293T cells stably expressing luciferase reporter construct driven by zebrafish *kif26ab* promoter were transfected with different amounts of CMV-Sinhcaf plasmid as indicated and luciferase activity was measured. Data shown are mean ± SEM (n = 3, biological replicates). Statistical analysis was performed using one-way ANOVA followed by Tukey's post hoc test. The different letters (a,b) indicate a significant difference between the means, P < 0.05.

demonstrate that *kif26ab* is transcriptionally activated by Sinhcaf. Our results indicate that Sinhcaf facilitates histone 3 deacetylation in the promoter region of *kif26ab* gene, which in turn maintains its maternal expression.

Kinesins have been shown to be responsible for the microtubule-dependent aggregation of germ plasm (Robb *et al*, 1996; Sinsimer *et al*, 2013; Campbell *et al*, 2015). Kif26ab, one member of the kinesin superfamily, can bind microtubules and has roles in cell signal transduction and facilitating termination of nociceptive responses by sequestering focal adhesion kinase (Zhou *et al*, 2009; Wang *et al*, 2018). To investigate whether decreased maternal mRNA levels of *kif26ab* is the reason for defective germ plasm aggregation in

MZ*sinhcaf*$^{-/-}$ embryos, the expression of *kif26ab* was suppressed through morpholino injection. Suppressed expression of *kif26ab* indeed resulted in defective germ plasm aggregation in cleavage furrows and decreased PGCs number in genital ridge. Injection of *kif26ab* mRNA could partly rescue the decreased germ plasm components in cleavage furrows of MZ*sinhcaf*$^{-/-}$ embryos. This led us to

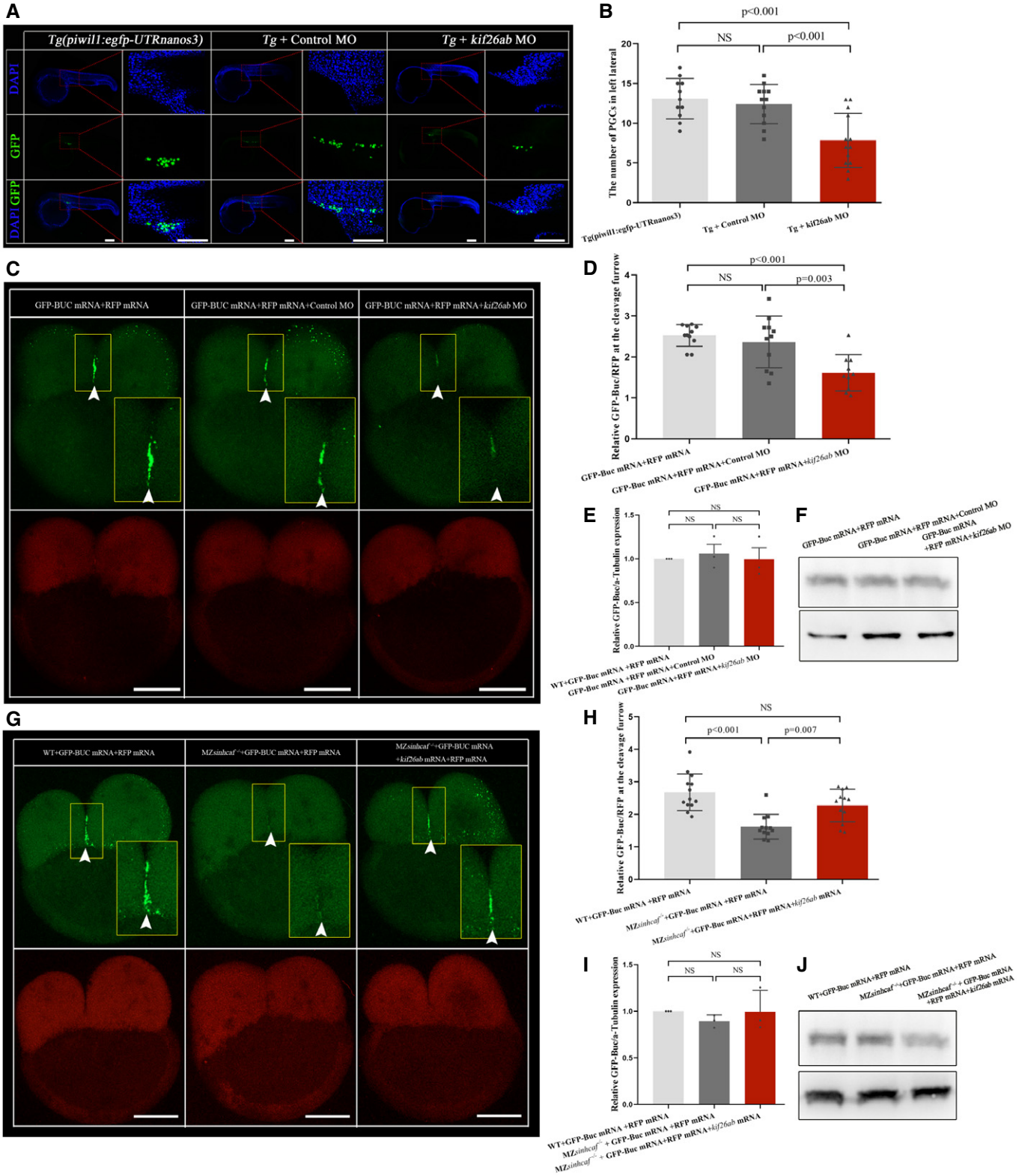

Figure 7.

Figure 7. The role of Sinhcaf in germ plasm aggregation and subsequent PGC specification is mediated by Kif26ab.

A Maximal intensity projection of a confocal z-stack of 24hpf *Tg(piwil:egfp)*, *Tg(piwil:egfp)* injected with *kif26ab* MO and *Tg(piwil:egfp)* injected with control MO embryos.

B Quantitative analysis of PGCs in 24hpf *Tg(piwil:egfp)* (n = 11), *Tg(piwil:egfp)* injected with *kif26ab* MO (n = 12) and *Tg(piwil:egfp)* injected with control MO (n = 13) embryos. Data shown are mean ± SEM (n = the number of embryos analyzed).

C Maximal intensity projection of a confocal z-stack of 4-cell stage embryos injected with GFP-Buc mRNA + RFP mRNA, GFP-Buc mRNA + RFP mRNA + Control MO and GFP-Buc mRNA + RFP mRNA + *kif26ab* MO. White arrowheads point to cleavage furrows of 4-cell embryos.

D Relative GFP-Buc density at the cleavage furrow of 4-cell stage embryos injected with GFP-Buc mRNA + RFP mRNA (n = 11), GFP-Buc mRNA + RFP mRNA + Control MO (n = 11) and GFP-Buc mRNA + RFP mRNA + *kif26ab* MO (n = 10). Data shown are mean ± SEM (n = the number of embryos analyzed).

E Statistical analysis of the relative levels of GFP-Buc/a-Tubulin. Data shown are mean ± SEM (n = 3, biological replicates).

F Western blots for GFP-Buc expression in 4-cell stage embryos injected with GFP-Buc mRNA + RFP mRNA, GFP-Buc mRNA + RFP mRNA + Control MO and GFP-Buc mRNA + RFP mRNA + *kif26ab* MO.

G Maximal intensity projection of a confocal z-stack of MZ*sinhcaf*$^{-/-}$ or WT 4-cell stage embryos injected with GFP-Buc mRNA + RFP mRNA or GFP-Buc mRNA + RFP mRNA + *kif26ab* mRNA. White arrowheads point to cleavage furrows of 4-cell embryos.

H Relative GFP-Buc density at the cleavage furrow of MZ*sinhcaf*$^{-/-}$ (n = 12) or WT (n = 13) 4-cell stage embryos injected with GFP-Buc mRNA + RFP mRNA or GFP-Buc mRNA + RFP mRNA + *kif26ab* mRNA. Data shown are mean ± SEM (n = the number of embryos analyzed).

I Statistical analysis of the relative levels of GFP-Buc/a-Tubulin. Data shown are mean ± SEM (n = 3, biological replicates).

J Western blots for GFP-Buc expression in MZ*sinhcaf*$^{-/-}$ or WT 4-cell stage embryos injected with GFP-Buc mRNA + RFP mRNA, GFP-Buc mRNA + RFP mRNA + Control MO and GFP-Buc mRNA + RFP mRNA + *kif26ab* MO.

Data information: Statistical analysis was performed using one-way ANOVA followed by Tukey's post hoc test. Scale bars, 100 μm.
Source data are available online for this figure.

establish a model for the roles of *sinhcaf*, transcription of *kif26ab* and germ plasm aggregation. In wild-type zebrafish, Sinhcaf promotes deacetylation of histone 3, which is essential for activating transcription of *kif26ab*. The critical role of Sinhcaf in germ plasm aggregation and subsequent PGC specification is mediated by Kif26ab (Fig 8A). Loss of Sinhcaf resulted in increased acetylation level of histone 3 in the promoter region of *kif26ab* and decreased level of Kif26ab, which is the reason for defective germ plasm aggregation and decreased number of PGCs in *sinhcaf* mutants (Fig 8B).

Histone deacetylation is involved in modulating the self-renewal and differentiation of pluripotent stem cells (Ware *et al*, 2009; Jamaladdin *et al*, 2014). PGCs are unipotent cells committed to germ lineage, while they will become pluripotent upon explantation in culture (Matsui *et al*, 1992; Resnick *et al*, 1992). Whether histone deacetylation process functions in self-renewal and differentiation of PGCs remains unclear. Our earlier work established that Sinhcafl, a homologous protein of Sinhcaf, is involved in reprogramming of somatic cell nuclear transfer (Luo *et al*, 2009; Hu *et al*, 2018). Here we found

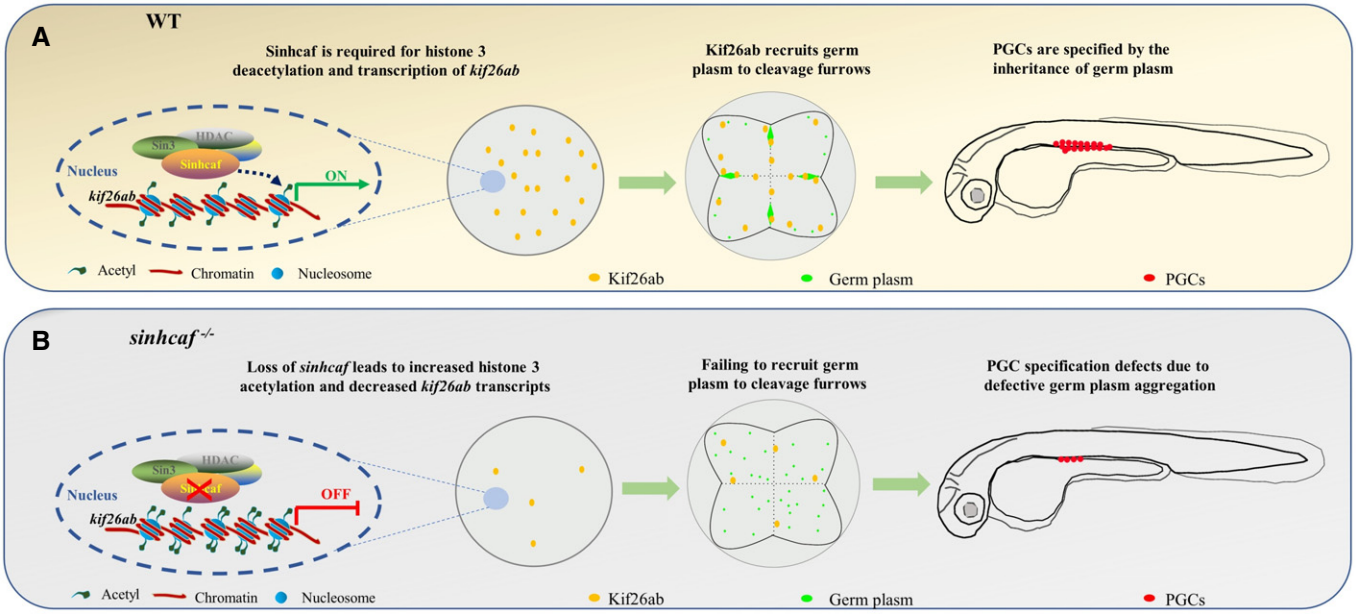

Figure 8. Model for the role of Sinhcaf in germ plasm aggregation and subsequent PGC specification is mediated by Kif26ab.

A Sinhcaf is the Sin3-HDAC complex associated factor. In WT eggs, Sinhcaf promotes deacetylation of histone 3, which is essential for activating transcription of *kif26ab*. In turn, Kif26ab promotes recruitment of germ plasm to furrows and subsequent PGC specification.

B In *sinhcaf*$^{-/-}$ eggs, transcription of *kif26ab* is blocked, resulting in failed germ plasm recruitment to specify PGCs.

Sinhcaf-mediated histone deacetylation modulates PGC specification. Our findings may open avenues for further investigating the role of histone deacetylation in self-renewal and differentiation of PGCs.

In summary, our results establish a critical role of Sinhcaf in germ plasm aggregation and subsequent PGC specification. Mechanistically, maternal *kif26ab* expression, which is essential for germ plasm aggregation in cleavage stage embryo, is regulated by Sinhcaf through erasing acetylation of histone in *kif26ab* promoter region directly. Our *sinhcaf*$^{-/-}$ mutants offer an amendable *in vivo* model system to determine what controls PGC specification. There are numerous reasons why this may be important, including manipulation of sex ratios, or to understand the role of histone deacetylation in self-renewal of germline stem cells (GSCs), which may aid in the search for fertility enhancers in humans.

Materials and Methods

Zebrafish care and maintenance

Zebrafish (*Danio rerio*) and their embryos were raised and maintained at 28.5°C. *Tg(piwil1:EGFP)* zebrafish of the AB genetic background were obtained from the China Zebrafish Resource Center (CZRC, Wuhan, China) (Ye *et al*, 2019). The density of fish is 50 larvae/l for age from 5 dpf to 15 dpf, 20 fish/l for age 15 dpf to 1 mpf, 10 fish/l for age from 1 mpf to 2 mpf, and 5 fish/l for age older than 2 mpf. Procedures involving zebrafish were approved by the Institutional Animal Care and Use Committee of the Institute of Hydrobiology, Chinese Academy of Sciences.

Establishment of transgenic and mutant zebrafish lines

To generate *Tg(CMV:EGFP;CMV:sinhcaf)* zebrafish, *sinhcaf* cDNA was ligated into the EcoRI/BclI site of the Tol2-CMV:EGFP-polyA-CMV:MCS-polyA-Tol2 vector. To generate *Tg(CMV: sinhcaf-EGFP)* zebrafish, *sinhcaf* ORF (without stop codon TGA) was ligated into the HindIII/SmaI site of the Tol2-CMV:MCS-EGFP-polyA-Tol2 vector. Prior to injection, Tol2-CMV:EGFP-polyA-CMV:MCS-polyA-Tol2 and Tol2-CMV:MCS-EGFP-polyA-Tol2 vectors were linearized with NotI, each linearized vector was co-injected with Tol2 mRNA into one-cell stage AB strain zebrafish embryos. The following days, embryos were monitored using a fluoroscope (Leica M250), only embryos displaying fluorescence were grown to adulthood and outcrossed with wild type to identify the founder fish. To generate *sinhcaf*$^{-/-}$ mutant zebrafish, the paired TALENs for *sinhcaf* gene were constructed using the golden gate method. TALEN mRNAs were synthesized using the mMessage mMACHINE SP6 Kit (Ambion, Inc., Austin, TX) and purified by LiCl precipitation. One-cell stage embryos were injected with TALEN mRNAs, injected embryos were raised to adulthood and then outcrossed with wild-type fish to identify founders that transmitted mutations through the germ line. Mutations were genotyped by competitive PCR and confirmed by sequencing.

Whole-mount in situ hybridization

Zebrafish *vasa, nanos3 and sinhcaf* cDNAs were cloned by PCR amplification and the products subcloned into the pCS2+ vector. Digoxigenin labeled antisense probes for *vasa, nanos3 and sinhcaf* were synthesized using T7 RNA Polymerase (Thermo Scientific) and DIG RNA Labeling Mix (Roche Diagnostics, Mannheim, Germany). Whole mount in situ hybridization was conducted as described by the Thisse Lab (Thisse & Thisse, 2008).

Whole-mount immunohistochemistry

Whole-mount immunohistochemistry was performed as described previously (Tao *et al*, 2018). Primary antibodies used were mouse anti-α-tubulin (1:1,000, Sigma T5168) and rabbit anti-phospho-myosin light chain 2 (p-NMII(Ser19), 1:50, CST 3671T). Goat anti-mouse-DyLight 549 IgG (1:500, Abbkine A23310-2) and goat anti-rabbit-Cy5 IgG (1:500, Bioss bs-0295G) were used as fluorescent secondary antibodies.

RT–PCR and RT–qPCR

Total RNA was extracted from zebrafish embryos, tissues, and ovarian follicles using TRIzol reagent (Invitrogen) and resuspended in nuclease-free water. The quality of extracted RNA was confirmed by UV spectrophotometer and agarose gel electrophoresis. Total RNA was reverse-transcribed into cDNA using ReverTra Ace qPCR RT Master Mix (TOYOBO). For RT–PCR, the cDNA samples were PCR-amplified using gene-specific primers as listed in Appendix Table S1. RT-qPCR was conducted with Roche LightCycler 480 real-time PCR system using 2×SYBR green real-time PCR mix (TOYOBO). *β-actin* was selected as a reference gene. 2-ΔΔCt method was used to calculate the relative expression levels of target genes against β-actin (Livak & Schmittgen, 2001). Primers used in RT–qPCR can be found in Appendix Table S2.

Embryo mounting, confocal microscopy, and image processing

Embryos were mounted in 0.5–1.0% low-melt agarose. Living embryos were anaesthetized in 168 mg/l tricaine before mounting. Fluorescence images were collected with laser scanning confocal microscope (Leica TCS SP5). Images were processed using Adobe Photoshop CS3 Extended. Fluorescence intensity was measured using ImageJ analysis software (NIH).

Co-immunoprecipitation

For immunoprecipitation assays in culture cells, full length of sinhcaf, sin3a, hdac1, and sap18 cDNAs were cloned into pEGFP-N1 or pCMV-HA vectors. HEK293T cells were transiently transfected with the indicated constructs of interest using Lipofectamine 3000 (Invitrogen, Thermo Fisher Scientific, Waltham, MA, USA) according to the manufacturer's instructions; 36 h after transfection, cells were harvested and lysed in RIPA buffer (Sangon Biotech, China) including protease inhibitors. Co-immunoprecipitation experiments were performed as previously described (van den Berg *et al*, 2010). Antibody against GFP (Abcam ab290, UK) and rabbit IgG (Beyotime Biotechnology A7016, China) were used.

Western blotting

Follicles of different stages were manually isolated and grouped as described previously (Poon *et al*, 2009). Total Protein Extraction Kit

(Sangon Biotech, China) was used to lyse different stage follicles. Total protein was electrophoresed on 12% SDS–PAGE gels and transferred to a polyvinylidene fluoride (PVDF) membrane, then probed with indicated primary antibodies against acetyl-histone H3 (K9 9649T), acetyl-histone H3 (K18 13998S), acetyl-histone H4 (K18 8647S) (all from Cell Signaling Technology), α-Tubulin (1:2,000, Sigma T9026), Histone H3 (1:1,000, Abcam ab1791) and EGFP (1:500, Abcam ab290). Signals were detected using Immobilon Western Chemiluminescent HRP Substrate (Merck-Millipore), and visualized using Image Quant LAS 4000 mini system (GE Healthcare). Immunoblots were analyzed with ImageJ (v1.48, NIH).

Bisulfite sequencing

Genomic DNA was isolated from WT and *sinhcaf*$^{-/-}$ follicles using the Universal Genomic DNA Kit (CWBiotech) following the manufacturer's protocol. The DNA (500–1,000 ng) was treated with bisulfite and purified with DNA Bisulfite Conversion Kit (TIANGEN, DP215) according to the manufacturer's protocol and was then subjected to PCR amplification with the following primers: *kif26ab*-bis-F 5′-GAGGTGGAGTTTTTTAAGGT-3′; *kif26ab*-bis-R 5′-ACCAA AACTAAAATACCCCT-3′. The amplified fragments were separated by agarose gel electrophoresis and the target bands were excised. Extracted gel bands were purified using Agarose Gel Extraction Kit and were subcloned into the pMD18-T vector. Randomly selected clones containing the target fragments of *kif26ab* were sequenced. Sequenced fragments were analyzed with the quantification tool for methylation analysis (http://quma.cdb.riken.jp).

Chromatin immunoprecipitation (ChIP)-qPCR

Chromatin immunoprecipitation assays were carried out using a variation of the protocol (https://wiki.zfin.org/display/prot/ZFIN+Protocol+Wiki). Briefly, to determine if a Sinhcaf-GFP fusion protein could bind to transcriptional regulatory region of *kif26ab* or *kif5bb*, about 600 36hpf embryos injected with 450 pg CMV-Sincaf-EGFP-SV40 polyA or CMV-RFP-EGFP-SV40 polyA were collected. Immunoprecipitation was carried out using ChIP Grade anti-EGFP antibody (Abcam ab290). To determine whether loss of *sinhcaf* affected the epigenetic status of the *kif26ab* gene, about 600 36hpf wild type or *sinhcaf* mutant embryos were collected. Immunoprecipitation was carried out using ChIP Grade anti- acetyl-histone H3 (K9 9649T) or acetyl-histone H3 (K18 13998S) antibodies. The relative amounts of *kif5bb* or *kif26ab* upstream region in immunoprecipitated chromatin and input control were measured using quantitative PCR with the respective gene primers. The primer sequences are listed in Appendix Table S3.

Chromatin immunoprecipitation (ChIP) -seq

About 600 36hpf wild type or MZ*sinhcaf* mutant embryos were used for acetyl-histone H3 (K9) ChIP-seq according to ChIP protocol described above. Library construction and bioinformatics analyses were performed by BGI (Shenzhen, China). The DNA is combined with End Repair Mix, and incubate at 20°C for 30 min. Purify the end-repaired DNA with QIAquick PCR Purification Kit (Qiagen), then add A-Tailing Mix, incubate at 37°C for 30 min. Combine the purified Adenylate 3′ Ends DNA, Adapter and Ligation Mix, incubate the ligation reaction at 20°C for 15 min. Purify the Adapter-ligated DNA with the QIAquick PCR Purification Kit. Several rounds of PCR amplification with PCR Primer Cocktail and PCR Master Mix are performed to enrich the Adapter-ligated DNA fragments. Then the PCR products are selected (about 100–300 bp, including adaptor sequence) by running a 2% agarose gel to recover the target fragments. Purify the gel with QIAquick Gel Extraction kit (QIAGEN). The final library was quantitated in two ways: determining the average molecule length and sample integrity as well as purity using the Agilent 2100 bioanalyzer instrument (Agilent DNA 1000 Reagents) and quantifying the library by real-time quantitative PCR (RT–qPCR). The sequencing was performed with the BGISEQ-500 sequencing system, featuring combinatorial probe-anchor synthesis (cPAS) and DNA Nanoballs (DNB) technology for superior data quality (BGI-Shenzhen, China). Raw reads were filtered first to remove low-quality or adaptor sequences by SOAPnuke with parameters: filter -l 5 -q 0.5 -n 0.1 -Q 2 −5 1 -c 50. Cleaned reads were mapped to the reference genome of GRCz11 using SOAPaligner/SOAP2 (version: 2.2.5), whose parameters is -v 2 -s 35. The different enrichment peaks from different samples was plotted by MAnorm (v1.1). The gene element annotation of peak or different enrichment peak from different samples was carried out by bedtools intersect mode with overlap 50%. To identify the characteristics of peaks, motif discovery was analyzed using HOMER (v4.10.3).

RNA sequencing

RNA sequencing was performed on five biological replicates for mature egg, four biological replicates for FG follicle of wild type and *sinhcaf*$^{-/-}$ zebrafish (18 total samples sequenced by Shanghai OE Biotech. Co., Ltd.). Each biological replicate was a pool of mature eggs or FG follicles from one female zebrafish. Total RNA was extracted using the mirVana miRNA Isolation Kit (Ambion) following the manufacturer's protocol. RNA integrity was evaluated using the Agilent 2100 Bioanalyzer (Agilent Technologies, Santa Clara, CA, USA). The samples with RNA Integrity Number (RIN) ≥ 7 were subjected to the subsequent analysis. The libraries were constructed using TruSeq Stranded mRNA LTSample Prep Kit (Illumina, San Diego, CA, USA) according to the manufacturer's instructions. Then these libraries were sequenced on the Illumina sequencing platform (HiSeq TM 2500 or Illumina HiSeq X Ten) and 125 bp/150 bp paired-end reads were generated. Raw data (raw reads) were processed using Trimmomatic v0.35. The reads containing ploy-N and the low-quality reads were removed to obtain the clean reads. These clean reads were mapped to reference genome using hisat2. FPKM value of each gene was calculated using cufflinks, and the read counts of each gene were obtained by htseq-count. DEGs were identified using the DESeq R package functions estimateSizeFactors and nbinomTest. $P < 0.05$ and fold Change > 2 or fold Change < 0.5 was set as the threshold for significantly differential expression. Hierarchical cluster analysis of DEGs was performed to explore genes expression pattern. Gene Ontology (GO) enrichment analysis of DEGs was performed using R, based on the hypergeometric distribution.

Luciferase-reporter assays

The zebrafish *kif26ab* promoter (1,707 bp) was amplified with the primers: *kif26ab*-F (KpnI) 5′-CGGGGTACCTTCCGTCGCCACAAAA CAAA-3′; *kif26ab*-R (HindIII) 5′-CCCAAGCTTATGGGCACCAGAG

CCCTTAG-3′. The promoter fragment was cloned into the pGL4 luciferase reporter plasmid (Promega). HEK293T cells stably expressing *kif26ab*-luciferase reporter construct were seeded at a density of 1.5×10^5 cells per well of a 12-well dish and cultured in complete DMEM (Gibco, USA) containing 10% FBS and maintained at 37°C and 5% CO_2. All transfections were performed with Lipofectamine 3000 (Invitrogen), according to manufacturer's instructions. Cells were harvested after 36 h, and the luciferase activity of the lysate was measured with the Dual-Luciferase reporter assay system (Promega, E1960) using SpectraMax i3 (Molecular Devices).

Knockdown experiments

The *kif26ab* specific antisense morpholino oligonucleotides (*kif26ab* MO 5′-CATGCGTTAAATCCATCATCTCGGT-3′), *kif5bb* specific antisense morpholino oligonucleotides (*kif5bb* MO 5′-CGCCATCT TCAGCTGTGAGGAGGAG-3′) and control morpholino oligonucleotides (Control MO 5′-CCTCTTACCTCAGTTACAATTTATA-3′) were designed and synthesized by Gene Tools (Philomath, OR, USA), dissolved to 1mM in nuclease-free water and stored at −20°C. For microinjection, MOs were diluted in 1×Danieau's buffer (58 mM NaCl, 0.7 mM KCl, 0.4 mM $MgSO_4$, 0.6 mM $Ca(NO3)_2$, 5 mM HEPES, pH 7.6) supplemented with phenol red. The effectiveness of the *kif26ab* MO and *kif5bb* MO were tested by co-injecting each MO with the pEGFP-N1 plasmid fused in frame with the MO target site.

Statistical analysis

Statistical analyses were conducted using GraphPad Prism 5 (GraphPad Software Inc.). Datasets were examined for normality and homogeneity of variance using the Shapiro–Wilk test and Levene's median test, respectively. Statistical analysis was performed using unpaired two-tailed Student's *t*-test, or one-way ANOVA followed by Tukey post hoc test, or 2-way ANOVA followed by Holm-Sidak post hoc test. Data are presented as mean ± SEM.

Data availability

All data, methods, and results of statistical analyses are reported in this paper. We welcome any specific inquiries.

- RNA-Seq data: Gene Expression Omnibus GSE159162 (https://www.ncbi.nlm.nih.gov/geo/query/acc.cgi?acc=GSE159162)
- ChIP-Seq data: Gene Expression Omnibus GSE198516 (https://www.ncbi.nlm.nih.gov/geo/query/acc.cgi?acc=GSE198516)

Expanded View for this article is available online.

Acknowledgments
The authors acknowledge with appreciation the help of Ms. Ming Li for care of animals and Ms Fang Zhou (Analytical & Testing Center, IHB, CAS) for providing confocal services. This work was supported by the National Natural Science Foundation of China (31721005, 31772833, and 32030113), the Chinese Academy of Sciences (Grant No. XDA24010108 and 152342KYSB20180019), the National Key R&D Program of China (2018YFD0901200), the Natural Science Foundation of Hubei Province (2020CFB381) and the Laboratory for Marine biology and Biotechnology (YQ2019NO04), Pilot National Laboratory for Marine Science and Technology (Qingdao). Funding from the University of Ottawa International Research Acceleration Program (to V.L.T. and W.H.) is acknowledged with appreciation.

Author contributions
Binbin Tao: Conceptualization; Data curation; Formal analysis; Investigation; Visualization; Methodology; Writing—original draft; Writing—review & editing. **Hongling Hu:** Conceptualization; Data curation; Formal analysis; Investigation; Visualization; Methodology. **Ji Chen:** Data curation; Formal analysis; Methodology. **Lu Chen:** Data curation; Investigation. **Daji Luo:** Formal analysis; Methodology. **Yonghua Sun:** Resources; Methodology. **Feng Ge:** Formal analysis; Methodology. **Zuo-yan Zhu:** Resources; Supervision. **Vance Trudeau:** Formal analysis; Supervision; Writing—review & editing. **Wei Hu:** Conceptualization; Resources; Formal analysis; Supervision; Funding acquisition; Writing—original draft; Writing—review & editing.

In addition to the CRediT author contributions listed above, the contributions in detail are:
BT: Conceptualization; Data curation; Formal analysis; Investigation; Visualization; Methodology; Writing—original draft; Writing—review and editing. HH: Conceptualization; Data curation; Formal analysis; Investigation; Visualization; Methodology. JC: Data curation; Formal analysis; Methodology. LC: Data curation; Investigation. DL: Formal Analysis; Methodology. YS: Resources; Methodology. FG: Formal Analysis; Methodology. ZZ: Resources; Supervision. VLT: Formal Analysis; Supervision; Writing—review and editing. WH: Conceptualization; Formal analysis; Resources; Supervision; Funding acquisition; Writing—original draft; Writing—review and editing.

Disclosure and competing interests statement
The authors declare that they have no conflict of interest.

References

Adams GE, Chandru A, Cowley SM (2018) Co-repressor, co-activator and general transcription factor: the many faces of the Sin3 histone deacetylase (HDAC) complex. *Biochem J* 475: 3921 – 3932

Agoulnik AI, Lu BS, Zhu QC, Truong C, Ty MT, Arango N, Chada KK, Bishop CE (2002) A novel gene, Pog, is necessary for primordial germ cell proliferation in the mouse and underlies the germ cell deficient mutation, gcd. *Hum Mol Genet* 11: 3047 – 3053

Akiyama T, Nagata M, Aoki F (2006) Inadequate histone deacetylation during oocyte meiosis causes aneuploidy and embryo death in mice. *Proc Natl Acad Sci USA* 103: 7339 – 7344

Barber MF, Michishita-Kioi E, Xi Y, Tasselli L, Kioi M, Moqtaderi Z, Tennen RI, Paredes S, Young NL, Chen K *et al* (2012) SIRT7 links H3K18 deacetylation to maintenance of oncogenic transformation. *Nature* 487: 114 – 118

van den Berg DLC, Snoek T, Mullin NP, Yates A, Bezstarosti K, Demmers J, Chambers I, Poot RA (2010) An Oct4-centered protein interaction network in embryonic stem cells. *Cell Stem Cell* 6: 369 – 381

Bontems F, Stein A, Marlow F, Lyautey J, Gupta T, Mullins MC, Dosch R (2009) Bucky ball organizes germ plasm assembly in zebrafish. *Curr Biol* 19: 414 – 422

Campbell PD, Heim AE, Smith MZ, Marlow FL (2015) Kinesin-1 interacts with Bucky ball to form germ cells and is required to pattern the zebrafish body axis. *Development* 142: 2996 – 3008

Chang YF, Imam JS, Wilkinson ME (2007) The nonsense-mediated decay RNA surveillance pathway. *Annu Rev Biochem* 76: 51 – 74

Cinalli RM, Rangan P, Lehmann R (2008) Germ cells are forever. *Cell* 132: 559 – 562

Colozza G, De Robertis EM (2014) Maternal syntabulin is required for dorsal axis formation and is a germ plasm component in Xenopus. *Differentiation* 88: 17 – 26

Dosch R, Wagner DS, Mintzer KA, Runke G, Wiemelt AP, Mullins MC (2004) Maternal control of vertebrate development before the midblastula transition: mutants from the zebrafish I. *Dev Cell* 6: 771 – 780

Dovey OM, Foster CT, Cowley SM (2010a) Emphasizing the positive A role for histone deacetylases in transcriptional activation. *Cell Cycle* 9: 2700 – 2701

Dovey OM, Foster CT, Cowley SM (2010b) Histone deacetylase 1 (HDAC1), but not HDAC2, controls embryonic stem cell differentiation. *Proc Natl Acad Sci USA* 107: 8242 – 8247

Eno C, Hansen CL, Pelegri F (2019) Aggregation, segregation, and dispersal of homotypic germ plasm RNPs in the early zebrafish embryo. *Dev Dynam* 248: 306 – 318

Eskandarian HA, Impens F, Nahori MA, Soubigou G, Coppee JY, Cossart P, Hamon MA (2013) A role for SIRT2-dependent histone H3K18 deacetylation in bacterial infection. *Science* 341: 1238858

Feng KE, Cui X, Song Y, Tao B, Chen JI, Wang J, Liu S, Sun Y, Zhu Z, Trudeau VL *et al* (2020) Gnrh3 regulates PGC proliferation and sex differentiation in developing zebrafish. *Endocrinology* 161: bqz024

Grieve KM, McLaughlin M, Dunlop CE, Telfer EE, Anderson RA (2015) The controversial existence and functional potential of oogonial stem cells. *Maturitas* 82: 278 – 281

Hashimoto Y, Maegawa S, Nagai T, Yamaha E, Suzuki H, Yasuda K, Inoue K (2004) Localized maternal factors are required for zebrafish germ cell formation. *Dev Biol* 268: 152 – 161

Hassig CA, Fleischer TC, Billin AN, Schreiber SL, Ayer DE (1997) Histone deacetylase activity is required for full transcriptional repression by mSin3A. *Cell* 89: 341 – 347

Hird SN, Paulsen JE, Strome S (1996) Segregation of germ granules in living *Caenorhabditis elegans* embryos: cell-type-specific mechanisms for cytoplasmic localisation. *Development* 122: 1303 – 1312

Houston DW, King ML (2000) A critical role for Xdazl, a germ plasm-localized RNA, in the differentiation of primordial germ cells in Xenopus. *Development* 127: 447 – 456

Hu HL, Tao BB, Chen J, Zhu ZY, Hu W (2018) Fam60al as a novel factor involved in reprogramming of somatic cell nuclear transfer in zebrafish (*Danio rerio*). *Int J Biol Sci* 14: 78 – 86

Illmensee K, Mahowald AP (1974) Transplantation of posterior polar plasm in *Drosophila* - induction of germ-cells at anterior pole of egg. *Proc Natl Acad Sci USA* 71: 1016 – 1020

Imamura M, Takahashi A, Yamauchi T, Hara K, Yasuda K, Grarup N, Zhao W, Wang XU, Huerta-Chagoya A, Hu C *et al* (2016) Genome-wide association studies in the Japanese population identify seven novel loci for type 2 diabetes. *Nat Commun* 7: 10531

Jamaladdin S, Kelly RDW, O'Regan L, Dovey OM, Hodson GE, Millard CJ, Portolano N, Fry AM, Schwabe JWR, Cowley SM (2014) Histone deacetylase (HDAC) 1 and 2 are essential for accurate cell division and the pluripotency of embryonic stem cells. *Proc Natl Acad Sci USA* 111: 9840 – 9845

Kao HY, Ordentlich P, Koyano-Nakagawa N, Tang Z, Downes M, Kintner CR, Evans RM, Kadesch T (1998) A histone deacetylase corepressor complex regulates the Notch signal transduction pathway. *Genes Dev* 12: 2269 – 2277

Karantzali E, Schulz H, Hummel O, Hubner N, Hatzopoulos A, Kretsovali A (2008) Histone deacetylase inhibition accelerates the early events of stem cell differentiation: transcriptomic and epigenetic analysis. *Genome Biol* 9: R65

Kistler KE, Trcek T, Hurd TR, Chen RC, Liang FX, Sall J, Kato M, Lehmann R (2018) Phase transitioned nuclear Oskar promotes cell division of *Drosophila* primordial germ cells. *Elife* 7: e37949

Krishnakumar P, Riemer S, Perera R, Lingner T, Goloborodko A, Khalifa H, Bontems F, Kaufholz F, El-Brolosy MA, Dosch R (2018) Functional equivalence of germ plasm organizers. *Plos Genet* 14: e1007696

Kurdistani SK, Robyr D, Tavazoie S, Grunstein M (2002) Genome-wide binding map of the histone deacetylase Rpd3 in yeast. *Nat Genet* 31: 248 – 254

Lee MT, Bonneau AR, Giraldez AJ (2014) Zygotic genome activation during the maternal-to-zygotic transition. *Annu Rev Cell Dev Bi* 30: 581 – 613

Lehmann R (2016) Germ plasm biogenesis-an Oskar-centric perspective. *Essays Dev Biol A* 116: 679 – 707

Li YX, Seto E (2016) HDACs and HDAC inhibitors in cancer development and therapy. *Csh Perspect Med* 6: a026831

Livak KJ, Schmittgen TD (2001) Analysis of relative gene expression data using real-time quantitative PCR and the 2(-Delta Delta C(T)) method. *Methods* 25: 402 – 408

Luo DJ, Hu W, Chen SP, Xiao Y, Sun YH, Zhu ZY (2009) Identification of differentially expressed genes between cloned and zygote-developing zebrafish (*Danio rerio*) embryos at the dome stage using suppression subtractive hybridization. *Biol Reprod* 80: 674 – 684

Marlow F (2015) Primordial germ cell specification and migration. *F1000Res* 4: 1462

Martin JJ, Woods DC, Tilly JL (2019) Implications and current limitations of oogenesis from female germline or oogonial stem cells in adult mammalian ovaries. *Cells-Basel* 8: 93

Matsuda KI, Mori H, Nugent BM, Pfaff DW, McCarthy MM, Kawata M (2011) Histone deacetylation during brain development is essential for permanent masculinization of sexual behavior. *Endocrinology* 152: 2760 – 2767

Matsui Y, Zsebo K, Hogan BLM (1992) Derivation of pluripotential embryonic stem-cells from murine primordial germ-cells in culture. *Cell* 70: 841 – 847

Munoz IM, MacArtney T, Sanchez-Pulido L, Ponting CP, Rocha S, Rouse J (2012) Family with sequence similarity 60A (FAM60A) protein is a cell cycle-fluctuating regulator of the SIN3-HDAC1 histone deacetylase complex. *J Biol Chem* 287: 32346 – 32353

Nabeshima R, Nishimura O, Maeda T, Shimizu N, Ide T, Yashiro K, Sakai Y, Meno C, Kadota M, Shiratori H *et al* (2018) Loss of Fam60a, a Sin3a subunit, results in embryonic lethality and is associated with aberrant methylation at a subset of gene promoters. *Elife* 7: e36435

Nair S, Marlow F, Abrams E, Kapp L, Mullins MC, Pelegri F (2013) The chromosomal passenger protein Birc5b organizes microfilaments and germ plasm in the zebrafish embryo. *Plos Genet* 9: e1003448

Poon SK, So WK, Yu XB, Liu L, Ge W (2009) Characterization of inhibin alpha subunit (inha) in the zebrafish: evidence for a potential feedback loop between the pituitary and ovary. *Reproduction* 138: 709 – 719

Raz E (2003) Primordial germ-cell development: the zebrafish perspective. *Nat Rev Genet* 4: 690 – 700

Resnick JL, Bixler LS, Cheng LZ, Donovan PJ (1992) Long-term proliferation of mouse primordial germ-cells in culture. *Nature* 359: 550 – 551

Riemer S, Bontems F, Krishnakumar P, Gomann J, Dosch R (2015) A functional Bucky ball-GFP transgene visualizes germ plasm in living zebrafish. *Gene Expr Patterns* 18: 44 – 52

Robb DL, Heasman J, Raats J, Wylie C (1996) A kinesin-like protein is required for germ plasm aggregation in Xenopus. *Cell* 87: 823 – 831

Saitou M, Yamaji M (2012) Primordial germ cells in mice. *Csh Perspect Biol* 4: a008375

Sinsimer KS, Lee JJ, Thiberge SY, Gavis ER (2013) Germ plasm anchoring is a dynamic state that requires persistent trafficking. *Cell Rep* 5: 1169 – 1177

Slanchev K, Stebler J, de la Cueva-Mendez G, Raz E (2005) Development without germ cells: the role of the germ line in zebrafish sex differentiation. *Proc Natl Acad Sci USA* 102: 4074 – 4079

Smith KT, Sardiu ME, Martin-Brown SA, Seidel C, Mushegian A, Egidy R, Florens L, Washburn MP, Workman JL (2012) Human family with sequence similarity 60 Member A (FAM60A) protein: a new subunit of the Sin3 deacetylase complex. *Mol Cell Proteomics* 11: 1815 – 1828

Streubel G, Fitzpatrick DJ, Oliviero G, Scelfo A, Moran B, Das S, Munawar N, Watson A, Wynne K, Negri GL *et al* (2017) Fam60a defines a variant Sin3a-Hdac complex in embryonic stem cells required for self-renewal. *EMBO J* 36: 2216 – 2232

Tao BB, Hu HL, Mitchell K, Chen J, Jia HB, Zhu ZY, Trudeau VL, Hu W (2018) Secretogranin-II plays a critical role in zebrafish neurovascular modeling. *J Mol Cell Biol* 10: 388 – 401

Theusch EV, Brown KJ, Pelegri F (2006) Separate pathways of RNA recruitment lead to the compartmentalization of the zebrafish germ plasm. *Dev Biol* 292: 129 – 141

Thisse C, Thisse B (2008) High-resolution in situ hybridization to whole-mount zebrafish embryos. *Nat Protoc* 3: 59 – 69

Tzung KW, Goto R, Saju JM, Sreenivasan R, Saito T, Arai K, Yamaha E, Hossain MS, Calvert MEK, Orban L (2015) Early depletion of primordial germ cells in zebrafish promotes testis formation. *Stem Cell Rep* 5: 156

Wang L, Tanaka Y, Wang DD, Morikawa M, Zhou RY, Homma N, Miyamoto Y, Hirokawa N (2018) The atypical Kinesin KIF26A facilitates termination of nociceptive responses by sequestering focal adhesion kinase. *Cell Rep* 24: 2894 – 2907

Wang ZB, Zang CZ, Cui KR, Schones DE, Barski A, Peng WQ, Zhao KJ (2009) Genome-wide mapping of HATs and HDACs reveals distinct functions in active and inactive genes. *Cell* 138: 1019 – 1031

Ware CB, Wang L, Mecham BH, Shen L, Nelson AM, Bar M, Lamba DA, Dauphin DS, Buckingham B, Askari B *et al* (2009) Histone deacetylase inhibition elicits an evolutionarily conserved self-renewal program in embryonic stem cells. *Cell Stem Cell* 4: 359 – 369

Ye D, Zhu L, Zhang QF, Xiong F, Wang HP, Wang XS, He MD, Zhu ZY, Sun YH (2019) Abundance of early embryonic primordial germ cells promotes zebrafish female differentiation as revealedby lifetime labeling of germline. *Mar Biotechnol* 21: 217 – 228

Yeung F, Hoberg JE, Ramsey CS, Keller MD, Jones DR, Frye RA, Mayo MW (2004) Modulation of NF-kappa B-dependent transcription and cell survival by the SIRT1 deacetylase. *EMBO J* 23: 2369 – 2380

Yoon C, Kawakami K, Hopkins N (1997) Zebrafish vasa homologue RNA is localized to the cleavage planes of 2- and 4-cell-stage embryos and is expressed in the primordial germ cells. *Development* 124: 3157 – 3165

Zhang HS, Gavin M, Dahiya A, Postigo AA, Ma DD, Luo RX, Harbour JW, Dean DC (2000) Exit from G1 and S phase of the cell cycle is regulated by repressor complexes containing HDAC-Rb-hSWI/SNF and Rb-hSWI/SNF. *Cell* 101: 79 – 89

Zhou RY, Niwa S, Homma N, Takei Y, Hirokawa N (2009) KIF26A is an unconventional kinesin and regulates GDNF-Ret signaling in enteric neuronal development. *Cell* 139: 802 – 813

Zimyanin VL, Belaya K, Pecreaux J, Gilchrist MJ, Clark A, Davis I, St Johnston D (2008) *In vivo* imaging of oskar mRNA transport reveals the mechanism of posterior localization. *Cell* 134: 843 – 853